

***Ab initio* Green's function formalism for band structures**

Christian Buth,* Uwe Birkenheuer, Martin Albrecht,† and Peter Fulde

Max-Planck-Institut für Physik komplexer Systeme, Nöthnitzer Straße 38, 01187 Dresden, Germany

(Received 3 September 2004; revised manuscript received 15 August 2005; published 17 November 2005)

Using the Green's function formalism, an *ab initio* theory for band structures of crystals is derived starting from the Hartree-Fock approximation. It is based on the algebraic diagrammatic construction scheme for the self-energy which is formulated for crystal orbitals (CO-ADC). In this approach, the poles of the Green's function are determined by solving a suitable Hermitian eigenvalue problem. The method is not only applicable to the outer valence and conduction bands, it is also stable for inner valence bands where strong electron correlations are effective. The key to the proposed scheme is to evaluate the self-energy in terms of Wannier orbitals before transforming it to a crystal momentum representation. Exploiting the fact that electron correlations are mainly local, one can truncate the lattice summations by an appropriate configuration selection scheme. This yields a flat configuration space; i.e., its size scales only linearly with the number of atoms per unit cell for large systems and, under certain conditions, the computational effort to determine band structures also scales linearly. As a first application of the new formalism, a lithium fluoride crystal has been chosen. A minimal basis set description is studied, and a satisfactory agreement with previous theoretical and experimental results for the fundamental band gap and the width of the F $2p$ valence band complex is obtained.

DOI: [10.1103/PhysRevB.72.195107](https://doi.org/10.1103/PhysRevB.72.195107)

PACS number(s): 71.10.-w, 71.15.Qe, 71.20.-b

I. INTRODUCTION

Band structures are of fundamental interest to the solid-state physicist as they reveal important properties of crystals.¹⁻⁶ The determination of band structures on *ab initio* level is therefore an important issue in theoretical solid-state physics. Nowadays predominantly density functional theory^{7,8} (DFT) with the local density approximation (LDA) or its variants are employed to treat this problem.^{3,4} DFT focuses on the ground-state electron density and yields ground-state properties. In several cases, the interpretation of the Kohn-Sham orbital energies as quasiparticle energies also turns out to be successful and particular attention has been paid to the LDA, due to its numerical simplicity. However, in insulating materials, the LDA tends to underestimate the band gap—e.g., Ref. 9.

As is well known, it is difficult to improve band structure calculations based on density functional theory. This is in particular the case when electron correlations are strong such that in quite some cases^{1,10-14} the one-electron picture becomes inappropriate and corrections are needed. Nevertheless, a number of ingenious methods have been devised to improve band structure results based on density functional theory. For example, the calculations have been supplemented by a GW treatment—e.g., Refs. 4, 15 and 16—or the so-called LDA+ U method.¹⁷ Other improvements concern the use of optimized effective potentials¹⁸ such as the exact exchange potential¹⁹ instead of its local, simplified form. Time-dependent DFT is another route to treat excited states more rigorously. Furthermore, LDA calculations have been coupled with various extensions of the coherent potential approximation (CPA) like the dynamical CPA^{20,21} or dynamical mean field theory (DMFT).²²⁻²⁷ Also Faddeev's method²⁸ of treating the three-particle t matrix has been applied in conjunction with LDA band structure calculations.²⁹ The same holds true for different forms of the projection operator technique.⁴ Yet one must face the fact that the various ap-

proximations remain uncontrolled and therefore have to be reconsidered from case to case.

When one is aiming at controlled approximations, two different routes offer themselves. One is bound to quantum Monte Carlo (QMC) calculations—e.g., Ref. 30. This is a simple and straightforward way of dealing with the many-body problem. Yet it suffers from one serious shortcoming, the so-called sign problem when treating fermions. Therefore, we are pursuing the second route. It starts from Hartree-Fock band structures and improves them by including correlations by means of many-particle techniques similar to the ones employed for molecules.^{4,6,31-41} Thereby one can take advantage of program packages like WANNIER which has been written by Shukla *et al.*^{42,43} or CRYSTAL which originates from Torino.^{2,5} Both provide Hartree-Fock bands as well as Wannier orbitals for crystals. These orbitals are especially suited for an *ab initio* treatment of electron correlations because of their local character.^{4,6}

A number of correlation calculations have been performed.^{4,6,31,35} A local Hamiltonian approach^{32-34,36,39,40} was shown to improve Hartree-Fock energy bands substantially. Suhai used Toyozawa's electronic polaron model⁴⁴ to repartition MP2 pair energies to estimate quasi-particle band structures.^{31,35,45-48} By inserting the orbital energies into the energy-dependent self-energy, this model was shown to be a special case of the outer valence Green's functions⁴⁹⁻⁵¹ (OVGFs) that were derived in terms of crystal orbitals by Liegener.^{31,35,48,52} By applying the approximation to the self-energy of Igarashi *et al.*,^{37,53} quasiparticle band structures were obtained by Albrecht *et al.*³⁷⁻³⁹

In the present paper, we derive the algebraic diagrammatic construction (ADC) scheme⁵⁴⁻⁵⁶ for crystals. The ADC scheme has proven to be superior to the OVGF method in molecular studies,⁵¹ and numerous works have been carried out over the last two decades—e.g., Refs. 12-14—including studies of oligomers and clusters chosen to model infinite chains or crystals.⁵⁷⁻⁵⁹ The ADC scheme is a method to ap-

proximate the Feynman-Dyson perturbation series for the self-energy and contains sums of certain proper and improper diagrams to infinite order.^{55,60,61} The basic properties of the ADC scheme and their derivations, as applied to molecules, are found in Refs. 62–64. Among those size extensivity is an important one since it is crucial when solids are considered. Furthermore, the ADC method is known to be robust and facilitates also to study strong electron correlations due to the efficient and stable evaluation of the one-particle Green's function in terms of a Hermitian eigenvalue problem. In molecules strong correlations for instance occur when inner valence electrons are treated.^{12–14} With the crystal orbital ADC (CO-ADC) devised here, the spectral representation of the one-particle Green's function is obtained. We suggest a formulation of the expressions in Wannier representation instead of crystal momentum representation in order to be able to exploit the local character of the correlation hole around an electron especially in the case of crystals with a large unit cell.

As a first application of the CO-ADC method to a three-dimensional crystalline solid, we have chosen lithium fluoride which occurs in nature as the mineral griceite. LiF not only has a wide range of technological applications like in x-ray monochromators or in filters for ultraviolet radiation—e.g., Ref. 65 (and references therein)—but is also interesting for a number of fundamental physical reasons. It is considered to be the “most ionic substance” and a prototypical insulator⁶⁵ which manifests in its very large fundamental band gap of¹⁶ 14.1 ± 0.1 eV that is the largest one found in nature apart from exotic systems. Some authors even consider LiF to be comparable to a He–Ne rare-gas solid.⁶⁵ Its optical spectra show strong excitonic effects, which complicates the experimental determination of the band gap⁶⁶ by optical spectroscopy. Similarly, many-particle effects have to be accounted for in the measurement of the widths of the F $2p$ and F $2s$ valence bands.

LiF has been thoroughly studied both experimentally and theoretically.^{38,39,43,65,67–73} Poole *et al.* survey early experimental and theoretical data.^{68,69} Recent studies of LiF comprise density functional theory calculations at the LDA level supplemented by an inclusion of correlation effects in terms of the GW approximation.^{15,65,73} *Ab initio* investigations comprise Hartree-Fock studies of ground-state properties^{43,71} and of the band structure.^{38,39,70} An accurate treatment of electron correlations for the ground-state properties of LiF (and other alkali halides) has been carried out by Doll and Stoll.⁷² Quasiparticle band structures have been obtained by Kunz⁷⁰ on the basis of the electronic polaron model⁴⁴ and by Albrecht³⁸ with the Green's function approach of Igarashi *et al.*⁵³

The article is structured as follows: Section II puts forward an *ab initio* foundation for band structures based on the one-particle Green's function. In Secs. III and IV, we derive the CO-ADC approximation to the self-energy in terms of Wannier orbitals. Section V combines the results of the previous sections to formulate the band structure problem as a Hermitian matrix eigenvalue problem. Criteria for the truncation of lattice sums are discussed in Sec. VI. In Sec. VII, the application of CO-ADC theory to lithium fluoride is described. Conclusions are drawn in Sec. VIII.

II. BAND STRUCTURES

The nonrelativistic Hamiltonian of a crystal in atomic units^{4,31,35} reads

$$\hat{H} = \sum_{n=1}^N \left[-\frac{1}{2} \Delta_n - \sum_{i=1}^{N_0} \sum_{A=1}^M \frac{Z_{R_i A}}{|\vec{r}_n - \vec{r}_{R_i A}|} \right] + \frac{1}{2} \sum_{\substack{m,n=1 \\ m \neq n}}^N \frac{1}{|\vec{r}_m - \vec{r}_n|} + \frac{1}{2} \sum_{\substack{i,j=1 \\ i \neq j \vee A \neq B}}^{N_0} \sum_{A,B=1}^M \frac{Z_{R_i A} Z_{R_j B}}{|\vec{r}_{R_i A} - \vec{r}_{R_j B}|}, \quad (1)$$

where fixed nuclei are assumed. Here N is the number of electrons in the crystal, N_0 denotes the number of unit cells, and M is the number of nuclei per unit cell. $Z_{R_i A} \equiv Z_A$ stands for the charge of nucleus A in unit cell \vec{R}_i , and $|\vec{r}_n - \vec{r}_{R_i A}|$ is the distance between the n th electron and the A th nucleus in unit cell \vec{R}_i . Finally, $|\vec{r}_m - \vec{r}_n|$ represents the distance between the m th and n th electron and $|\vec{r}_{R_i A} - \vec{r}_{R_j B}|$ denotes the distance between the nuclei A, B of charge $Z_{R_i A} \equiv Z_A, Z_{R_j B} \equiv Z_B$ in unit cells \vec{R}_i, \vec{R}_j .

The Schrödinger equation with the Hamiltonian (1) can be solved for the ground state in a restricted, closed-shell Hartree-Fock approximation,^{10,11,74–76} yielding a set of spin Bloch orbitals $\psi_{\vec{k}p}(\vec{r})$ where \vec{k} is the crystal momentum and p is a band index.^{1–5,10,11,74–76} We use these orbitals to represent the Hamiltonian (1) in second quantization, yielding the so-called Bloch or crystal momentum representation.³ It is decomposed according to Møller and Plesset^{77–79} into the Hartree-Fock part $\hat{H}_{\text{HF}}^{\text{BF}}$ and the residual interaction $\hat{H}_{\text{res}}^{\text{BF}}$, a suitable form to apply perturbation theory:

$$\hat{H} = \hat{H}_{\text{HF}}^{\text{BF}} + \hat{H}_{\text{res}}^{\text{BF}},$$

$$\hat{H}_{\text{HF}}^{\text{BF}} = \sum_{\vec{k}p} \varepsilon_{\vec{k}p} \hat{c}_{\vec{k}p}^\dagger \hat{c}_{\vec{k}p},$$

$$\hat{H}_{\text{res}}^{\text{BF}} = \sum_{\vec{k}_1 p, \vec{k}_2 q} W_{\vec{k}_1 p, \vec{k}_2 q} \hat{c}_{\vec{k}_1 p}^\dagger \hat{c}_{\vec{k}_2 q} + \frac{1}{2} \sum_{\substack{\vec{k}_1 p, \vec{k}_2 q, \\ \vec{k}_3 r, \vec{k}_4 s}} V_{\vec{k}_1 p, \vec{k}_2 q, \vec{k}_3 r, \vec{k}_4 s} \times \hat{c}_{\vec{k}_1 p}^\dagger \hat{c}_{\vec{k}_2 q}^\dagger \hat{c}_{\vec{k}_4 s} \hat{c}_{\vec{k}_3 r}, \quad (2)$$

The energy bands (or Bloch orbital energies) are denoted by $\varepsilon_{\vec{k}p}$, and the operators $\hat{c}_{\vec{k}p}^\dagger$ ($\hat{c}_{\vec{k}p}$) create (annihilate) electrons in $\psi_{\vec{k}p}(\vec{r})$. The negative of the Hartree-Fock potential is given by $W_{\vec{k}_1 p, \vec{k}_2 q} = -\sum_{\vec{k}_i} V_{\vec{k}_1 p, \vec{k}_i} [\vec{k}_2 q \vec{k}_i] n_{\vec{k}_i}$, the occupation numbers $n_{\vec{k}p}$ being unity for occupied and zero for unoccupied (or virtual) Bloch orbitals (and $\bar{n}_{\vec{k}p} = 1 - n_{\vec{k}p}$). Generally, we use the band indices i, j, m, n, \dots to denote occupied Hartree-Fock bands, a, b, c, d, \dots for unoccupied bands, and p, q, r, s, \dots for bands which are occupied or unoccupied. The two-electron integrals in Eq. (2) are defined with respect to Bloch orbitals by^{77–79}

$$V_{\vec{k}_1 p \vec{k}_2 q \vec{k}_3 r \vec{k}_4 s} = \int \int \psi_{\vec{k}_1 p}^\dagger(\vec{r}_1) \psi_{\vec{k}_2 q}^\dagger(\vec{r}_2) \frac{1}{|\vec{r}_1 - \vec{r}_2|} \times \psi_{\vec{k}_3 r}(\vec{r}_1) \psi_{\vec{k}_4 s}(\vec{r}_2) d^3 r_1 d^3 r_2. \quad (3)$$

The antisymmetrized two-electron integrals are

$$V_{\vec{k}_1 p \vec{k}_2 q [\vec{k}_3 r \vec{k}_4 s]} = V_{\vec{k}_1 p \vec{k}_2 q \vec{k}_3 r \vec{k}_4 s} - V_{\vec{k}_1 p \vec{k}_2 q \vec{k}_4 s \vec{k}_3 r} \quad (4)$$

and consist of a Coulomb term $V_{\vec{k}_1 p \vec{k}_2 q \vec{k}_3 r \vec{k}_4 s}$ and an exchange term $V_{\vec{k}_1 p \vec{k}_2 q \vec{k}_4 s \vec{k}_3 r}$. All crystal momentum vectors in Eqs. (2)–(4) are restricted to the first Brillouin zone. Furthermore, we assume that the first Brillouin zone is discretized by the Born–von Kármán boundary conditions or, equivalently, that numerical integrations in reciprocal space are carried out in terms of a Monkhorst-Pack net.^{2,5,80} In both cases, integrations over the Brillouin zone are approximated by finite sums.

The one-particle Green's function (or particle propagator) in terms of Bloch orbitals^{3,55,81–83} reads

$$G_{\vec{k} p \vec{k}' q}(t, t') = (-i) \langle \Psi_0^N | \hat{T} [\hat{c}_{\vec{k} p}(t) \hat{c}_{\vec{k}' q}^\dagger(t')] | \Psi_0^N \rangle, \quad (5)$$

with Wick's time-ordering operator \hat{T} . $|\Psi_0^N\rangle$ is the exact ground state of the N -particle system. Due to translational symmetry of the Hamiltonian (1), the one-particle Green's function depends only on one crystal momentum³—i.e., $G_{\vec{k} p \vec{k}' q}(t, t') = \delta_{\vec{k}, \vec{k}'} G_{p q}(\vec{k}, t, t')$.

Similarly, the time independence of the Hamiltonian (1) causes the particle propagator (5) to depend only on the time difference $t - t'$.^{81–83} Fourier transforming $G_{p q}(\vec{k}, t - t')$ with respect to $t - t'$ yields the one-particle Green's function in energy space $G_{p q}(\vec{k}, \omega)$ which can be recast in terms of the spectral or Lehmann representation as^{81–83}

$$G_{p q}(\vec{k}, \omega) = \sum_{n \in \{N+1\}} \frac{y_p^{(n)}(\vec{k}) y_q^{(n)*}(\vec{k})}{\omega + A_n(\vec{k}) + i\eta} + \sum_{n \in \{N-1\}} \frac{x_p^{(n)}(\vec{k}) x_q^{(n)*}(\vec{k})}{\omega + I_n(\vec{k}) - i\eta} \quad (6a)$$

$$= G_{p q}^+(\vec{k}, \omega) + G_{p q}^-(\vec{k}, \omega). \quad (6b)$$

Here n numerates the excited states of the $(N \pm 1)$ -particle system. The negative of the pole positions in Eq. (6a) is given by either the electron affinities $A_n(\vec{k}) = E_0^N - E_n^{N+1}(\vec{k})$ or the ionization potentials $I_n(\vec{k}) = E_n^{N-1}(-\vec{k}) - E_0^N$ where $E_n^{N \pm 1}(\pm \vec{k})$ are the energies of the different excited states of the $(N \pm 1)$ -particle system. The summands $\pm i\eta$ are required to ensure the convergence of the Fourier transformation. Whenever such a factor occurs, we implicitly take the limit $\eta \rightarrow 0^+$.^{81–83}

The pole strengths in Eq. (6a) are given by the transition amplitudes⁸⁴

$$y_p^{(n)}(\vec{k}) = \langle \Psi_0^N | \hat{c}_{\vec{k} p} | \Psi_n^{N+1}(\vec{k}) \rangle, \quad x_p^{(n)}(\vec{k}) = \langle \Psi_n^{N-1}(-\vec{k}) | \hat{c}_{\vec{k} p} | \Psi_0^N \rangle, \quad (7)$$

where $|\Psi_n^{N \pm 1}(\pm \vec{k})\rangle$ denote excited states of the $(N \pm 1)$ -particle system with crystal momenta $\pm \vec{k}$. The pole strengths can be

interpreted in terms of the spectral intensities observed in photoelectron spectroscopy experiments, similarly to the molecular case discussed in Ref. 50.

To obtain electron affinities and ionization potentials from the band structure of three-dimensional crystals, one has to specify the energy of the added (removed) electron at the Fermi level of the neutral crystal.^{85,86} This is usually done by introducing chemical potentials μ^\pm which are added to the pole positions of the one-particle Green's function—i.e., $A_n(\vec{k}) + \mu^+$ and $I_n(\vec{k}) + \mu^-$.

The (fundamental) band gap is the smallest difference between the energies for removing an electron from and attaching an electron to an N -particle system:

$$E_{\text{gap}} = (E^{N-1} - E_0^N) - (E_0^N - E^{N+1}) = I - \mu^- - A + \mu^+. \quad (8)$$

Here A stands for the largest electron affinity and I designates its smallest ionization potential. Correspondingly, $E^{N \pm 1}$ denote the energies of the electron attachment (removal) state with the lowest (highest) energy and E_0^N represents the ground-state energy.

The self-energy $\Sigma(\vec{k}, \omega)$ with respect to the residual interaction $\hat{H}_{\text{res}}^{\text{BF}}$ is defined by the Dyson equation^{3,55,81–83}

$$\begin{aligned} \mathbf{G}(\vec{k}, \omega) &= \mathbf{G}^0(\vec{k}, \omega) + \mathbf{G}^0(\vec{k}, \omega) \Sigma(\vec{k}, \omega) \mathbf{G}(\vec{k}, \omega) \\ &= \mathbf{G}^0(\vec{k}, \omega) + \mathbf{G}^0(\vec{k}, \omega) \Sigma(\vec{k}, \omega) \mathbf{G}^0(\vec{k}, \omega) + \dots, \end{aligned} \quad (9a)$$

which can be solved formally by

$$\mathbf{G}(\vec{k}, \omega) = [\mathbf{G}^0(\vec{k}, \omega)^{-1} - \Sigma(\vec{k}, \omega)]^{-1}, \quad (10)$$

where

$$G_{p q}^0(\vec{k}, \omega) = \delta_{\vec{k} p, \vec{k} q} \left[\frac{\bar{n}_{\vec{k} p}}{\omega - \varepsilon_{\vec{k} p} + i\eta} + \frac{n_{\vec{k} p}}{\omega - \varepsilon_{\vec{k} p} - i\eta} \right] \quad (11)$$

is the free Green's function with respect to the Møller-Plesset partition (2). In fact, for crystals with a band gap, the occupation numbers in Eq. (11) are independent of \vec{k} —i.e., $n_{\vec{k} p} = n_p$ and $\bar{n}_{\vec{k} p} = \bar{n}_p$.

The self-energy can be decomposed into an ω -independent part, the static self-energy $\Sigma^\infty(\vec{k})$, and an ω -dependent part, the dynamic self-energy $\mathbf{M}(\vec{k}, \omega)$,^{50,55,87,88}

$$\Sigma(\vec{k}, \omega) = \Sigma^\infty(\vec{k}) + \mathbf{M}(\vec{k}, \omega), \quad (12)$$

where $\lim_{\omega \rightarrow \pm\infty} \mathbf{M}(\vec{k}, \omega) = \mathbf{0}$. The dynamic self-energy is considered first in the ensuing Sec. III as the static self-energy is determined using the former one in Sec. IV.

III. DYNAMIC SELF-ENERGY

A. Crystal momentum representation

The partition (2) of the Hamiltonian has the same form and meaning as the Møller-Plesset partition for canonical molecular orbitals^{77–79} used frequently in molecular physics.

Therefore, all equations derived on the basis of the molecular Møller-Plesset partition are in complete analogy to the equations in the crystalline case. The only difference between molecules and crystals is the occurrence of composite indices in the Hamiltonian (2), consisting of a crystal momentum vector \vec{k} and a band index p which vary independently. Given an equation in terms of molecular orbitals, it can be written immediately in terms of Bloch orbitals by replacing all molecular orbital indices by composite indices. Afterwards one can exploit (translational) symmetry to simplify the equation.

The dynamic self-energy $M(\vec{k}, \omega)$ is represented in terms of the $2p1h/2h1p$ propagator (two-particle-one-hole–two-hole-one-particle-propagator) and possesses the spectral representation^{55,87,88}

$$\begin{aligned} M_{pq}(\vec{k}, \omega) &= \sum_{n \in \{N+1\}} \frac{m_p^{+, (n)}(\vec{k}) m_q^{+, (n)*}(\vec{k})}{\omega - \omega_n^+(\vec{k}) + i\eta} \\ &+ \sum_{n \in \{N-1\}} \frac{m_p^{-, (n)}(\vec{k}) m_q^{-, (n)*}(\vec{k})}{\omega - \omega_n^-(\vec{k}) - i\eta} \\ &= M_{pq}^+(\vec{k}, \omega) + M_{pq}^-(\vec{k}, \omega), \end{aligned} \quad (13)$$

where $\omega_n^\pm(\vec{k})$ denote the pole positions of the $2p1h/2h1p$ propagator and the $m_p^{\pm, (n)}(\vec{k})$ are termed Dyson amplitudes. The retarded dynamic self-energy $M_{pq}^+(\vec{k}, \omega)$ and the advanced dynamic self-energy $M_{pq}^-(\vec{k}, \omega)$ are associated with excitations of the $(N \pm 1)$ -particle system, respectively. Yet the pole positions $\omega_n^\pm(\vec{k})$ do *not* directly correspond to the energies of physical states as the (dynamic) self-energy is only defined in conjunction with the Dyson equation (9).

The algebraic diagrammatic construction scheme is a stable and efficient method to determine the spectral representation of the dynamic self-energy (13). The construction starts by making the ansatz

$$M_{pq}^\pm(\vec{k}, \omega) = \vec{U}_p^{\pm\dagger}(\vec{k}) [\omega \mathbb{1} - \mathbf{K}^\pm(\vec{k}) - \mathbf{C}^\pm(\vec{k})]^{-1} \vec{U}_q^\pm(\vec{k}), \quad (14)$$

which is termed general algebraic form or ADC form. The vectors $\vec{U}_q^\pm(\vec{k})$ are called modified coupling amplitudes for the crystal orbital $\vec{k}q$. Both $\mathbf{K}^\pm(\vec{k})$ and $\mathbf{C}^\pm(\vec{k})$ are Hermitian matrices, $\mathbf{C}^\pm(\vec{k})$ being referred to as modified interaction matrices,⁵⁵ while $\mathbf{K}^\pm(\vec{k})$ are assumed to be diagonal. Explicit expressions for these matrices are given below in Eq. (18).

The ADC form (14) reproduces the analytic structure of the Feynman-Dyson perturbation series for the dynamic self-energy as can be seen from its expansion into a geometric series:

$$\begin{aligned} M_{pq}^\pm(\vec{k}, \omega) &= \vec{U}_p^{\pm\dagger}(\vec{k}) \sum_{n=0}^{\infty} [(\omega \mathbb{1} - \mathbf{K}^\pm(\vec{k}))^{-1} \mathbf{C}^\pm(\vec{k})]^n \\ &\times (\omega \mathbb{1} - \mathbf{K}^\pm(\vec{k}))^{-1} \vec{U}_q^\pm(\vec{k}). \end{aligned} \quad (15)$$

The n th-order approximation to the ADC form (14) is constructed by inserting the perturbation expansions

$$\mathbf{U}^\pm(\vec{k}) = \mathbf{U}^{\pm(1)}(\vec{k}) + \mathbf{U}^{\pm(2)}(\vec{k}) + \dots,$$

$$\mathbf{C}^\pm(\vec{k}) = \mathbf{C}^{\pm(1)}(\vec{k}) + \mathbf{C}^{\pm(2)}(\vec{k}) + \dots, \quad (16)$$

in terms of the residual interaction $\hat{H}_{\text{res}}^{\text{BF}}$ into Eq. (15), and comparing the resulting expressions with the diagrammatic expansion of the dynamic self-energy up to n th order. This constitutes a scheme which is denoted by ADC(n). Note that the analytic structure imposed by Eq. (15) occasionally requires one to associate linear combinations of the analytic expression of several diagrams with particular terms in the above expansion.

In ADC(2) and ADC(3), each entry of the $\vec{U}_q^\pm(\vec{k})$ and the $\mathbf{K}^\pm(\vec{k}) + \mathbf{C}^\pm(\vec{k})$ in Eq. (14) is characterized by one or two, respectively, arrangements of two particles and one hole ($2p1h$) for $M_{pq}^+(\vec{k}, \omega)$ and two holes and one particle ($2h1p$) for $M_{pq}^-(\vec{k}, \omega)$. In brief notation these arrangements are referred to as $2p1h$ and $2h1p$ configurations. All such configurations that can be formed with the one-particle basis set underlying a Hartree-Fock calculation constitute the configuration space in ADC(2) and ADC(3). The configuration space is enlarged in ADC(4) by $3p2h$ and $3h2p$ configurations.⁵⁵ In general, every second order in ADC, the configuration space enlarges by the next higher excitation class. Restricting our discussion to $2p1h$ and $2h1p$ configurations, we can rewrite Eq. (14) as

$$\begin{aligned} M_{pq}^+(\vec{k}, \omega) &= \sum'_{\substack{\vec{l}_1, \vec{l}_2, \vec{l}'_1, \vec{l}'_2 \\ i, a, b, i', a', b'}} U_{\vec{k}}^{+*}{}_{p: \vec{l}_1 + \vec{l}_2 - \vec{k} \ i \ \vec{l}_1 \ \vec{l}_2 b} \\ &\times [\omega \mathbb{1} - \mathbf{K}^+(\vec{k}) - \mathbf{C}^+(\vec{k})]_{\vec{l}_1 + \vec{l}_2 - \vec{k} \ i \ \vec{l}_1 \ \vec{l}_2 b}^{-1} \\ &\quad \vec{l}'_1 + \vec{l}'_2 - \vec{k} \ i' \ \vec{l}'_1 a' \ \vec{l}'_2 b'} \\ &\times U_{\vec{k}}^{+}{}_{q: \vec{l}'_1 + \vec{l}'_2 - \vec{k} \ i' \ \vec{l}'_1 a' \ \vec{l}'_2 b'}. \end{aligned} \quad (17)$$

The prime on the summation symbol indicates that the summation only runs over indices with $\vec{l}_1 a < \vec{l}_2 b$ and $\vec{l}'_1 a' < \vec{l}'_2 b'$ to avoid double counting of contributions. The corresponding ansatz for $M^-(\vec{k}, \omega)$ is formally identical to Eq. (17) apart from the changed occupation numbers of the band indices $i \rightarrow a$, $a \rightarrow i$, $b \rightarrow j$, $i' \rightarrow a'$, $a' \rightarrow i'$, and $b' \rightarrow j'$. The summation variables \vec{l}_1 , \vec{l}_2 , \vec{l}'_1 , and \vec{l}'_2 are crystal momentum vectors like \vec{k} . The quantities $M^\pm(\vec{k}, \omega)$, $\mathbf{U}^\pm(\vec{k})$, $\mathbf{K}^\pm(\vec{k})$, and $\mathbf{C}^\pm(\vec{k})$ are invariant under translations by an arbitrary lattice vector, a property which is taken into account for the internal summations in the ADC form (17).

Explicit molecular ADC equations up to fourth order are given in Ref. 55. Here we show only the ADC equations for the dynamic self-energy in terms of crystal (Bloch) orbitals up to second order [CO-ADC(2)]:

$$U_{\vec{k}}^{+}{}_{p: \vec{l}_1 + \vec{l}_2 - \vec{k} \ i \ \vec{l}_1 \ \vec{l}_2 b} = V_{\vec{k}}^{+*}{}_{p \ \vec{l}_1 + \vec{l}_2 - \vec{k} \ i | \vec{l}_1 a \ \vec{l}_2 b} n_{\vec{l}_1 + \vec{l}_2 - \vec{k} \ i} \bar{n}_{\vec{l}_1 a} \bar{n}_{\vec{l}_2 b}, \quad (18a)$$

$$\begin{aligned}
 K_{\vec{l}_1+\vec{l}_2-\vec{k} \ i \ \vec{l}_1 a \ \vec{l}_2 b}^+ &= \delta_{\vec{l}_1+\vec{l}_2-\vec{k} \ i \ \vec{l}_1 a \ \vec{l}_2 a} (\varepsilon_{\vec{l}_1 a}^+ + \varepsilon_{\vec{l}_2 b}^- - \varepsilon_{\vec{l}_1+\vec{l}_2-\vec{k} \ i}^-) \\
 &\quad \frac{\bar{l}_1+\vec{l}_2-\vec{k} \ i \ \vec{l}_1 a' \ \vec{l}_2 b'}{\bar{l}_1+\vec{l}_2-\vec{k} \ i \ \vec{l}_1 a' \ \vec{l}_2 b'} \\
 &\quad \times n_{\vec{l}_1+\vec{l}_2-\vec{k} \ i} \bar{n}_{\vec{l}_1 a} \bar{n}_{\vec{l}_2 b}, \quad (18b)
 \end{aligned}$$

$$\begin{aligned}
 C_{\vec{l}_1+\vec{l}_2-\vec{k} \ i \ \vec{l}_1 a \ \vec{l}_2 b}^+ &= 0. \quad (18c) \\
 &\quad \frac{\bar{l}_1+\vec{l}_2-\vec{k} \ i \ \vec{l}_1 a' \ \vec{l}_2 b'}{\bar{l}_1+\vec{l}_2-\vec{k} \ i \ \vec{l}_1 a' \ \vec{l}_2 b'}
 \end{aligned}$$

The equations for $U^-(\vec{k})$, $K^-(\vec{k})$, and $C^-(\vec{k})$ are formally identical to Eq. (18) apart from the change of labels as for the adaptation of Eq. (17) to $M_{pq}^-(\vec{k}, \omega)$ and the occupation numbers in Eqs. (18a) and (18b) which are in this case $\bar{n}_{\vec{l}_1+\vec{l}_2-\vec{k} \ a} n_{\vec{l}_1 i} n_{\vec{l}_2 j}$. Expression (18) is derived in Ref. 89 utilizing a Gaussian basis set expansion of the Bloch orbitals.

The spectral representation (13) of the dynamic self-energy is obtained from the ADC form (14) by solving the Hermitian eigenvalue problem

$$\begin{aligned}
 [K^\pm(\vec{k}) + C^\pm(\vec{k})]Y^\pm(\vec{k}) &= Y^\pm(\vec{k})\Omega^\pm(\vec{k}), \\
 Y^{\pm\dagger}(\vec{k})Y^\pm(\vec{k}) &= 1. \quad (19)
 \end{aligned}$$

The vector notation in Eqs. (14) and (19) is a convenient means to sum over all intermediate crystal momenta and band indices. The diagonal matrix $\Omega^\pm(\vec{k})$ contains the eigenvalues of the secular matrix $K^\pm(\vec{k}) + C^\pm(\vec{k})$, and $Y^\pm(\vec{k})$ denotes the eigenvector matrix. The eigenvalues are the pole positions of the dynamic self-energy—i.e., $\omega_n^\pm(\vec{k}) = \Omega_{nm}^\pm(\vec{k})$ —while the Dyson amplitudes in Eq. (13) are obtained via

$$m_p^{\pm, (n)}(\vec{k}) = \bar{U}_p^{\pm\dagger}(\vec{k}) \bar{Y}^{\pm, (n)}(\vec{k}), \quad (20)$$

where the n th column vector $\bar{Y}^{\pm, (n)}(\vec{k})$ of $Y^\pm(\vec{k})$ is used here together with the adjoint of $\bar{U}_p^\pm(\vec{k})$. Note that, unlike CO-ADC(2), in CO-ADC(3) (and higher orders) the eigenvectors $\bar{Y}^{\pm, (n)}(\vec{k})$ couple several $2p1h$, $2h1p$, or higher excited configurations via the modified coupling amplitudes (18c) which are nonzero in this case.

B. Wannier representation

We derive in the following an expansion of the dynamic self-energy in terms of generalized Wannier orbitals; such orbitals are localized within unit cells and allow one to apply cutoff criteria inside a cell and between a cell and other cells. This affords one the ability to apply fine-grained configuration selection which is independent of the actual choice of the unit cell. In particular, it enables the treatment of crystals with large unit cells, not amenable to Bloch-orbital-based approaches (Sec. VI).^{4,6,31,35}

The generalized Wannier transformation^{1,3,31,35,90-92} and its inverse which mediate between Bloch and Wannier orbitals are

$$w_{R\varrho}(\vec{r}) = \frac{1}{\sqrt{N_0}} \sum_{\vec{k}} \sum_{p=1}^K \mathcal{U}_{p\varrho}(\vec{k}) e^{-i\vec{k}\cdot\vec{r}} \psi_{\vec{k}p}(\vec{r}), \quad (21a)$$

$$\psi_{\vec{k}p}(\vec{r}) = \frac{1}{\sqrt{N_0}} \sum_{\vec{R}} \sum_{\varrho=1}^K \mathcal{U}_{p\varrho}^*(\vec{k}) e^{i\vec{k}\cdot\vec{R}} w_{\vec{R}\varrho}(\vec{r}), \quad (21b)$$

where K denotes the number of bands involved in the transformation and $\mathcal{U}(\vec{k})$ is a suitable unitary matrix as generated, e.g., by the localization procedures in Refs. 91 and 92. Both Bloch and Wannier orbitals are normalized to unity upon integration over the entire crystal which consists of N_0 unit cells. Generally, we denote the Wannier orbital indices that result from occupied bands with $\kappa, \lambda, \mu, \nu, \dots$, while the Wannier orbital indices of unoccupied bands are denoted by $\alpha, \beta, \gamma, \delta, \dots$. Indices of Wannier orbitals from occupied or unoccupied bands are referred to by $\rho, \sigma, \tau, \nu, \dots$.

For an evaluation of the one-particle Green's function in terms of the Feynman-Dyson perturbation series, it is essential that there is no mixing between occupied and virtual Wannier orbitals; otherwise Wick's theorem can no longer be applied.⁸¹⁻⁸³ To fulfill this requirement, the Wannier transformation (21a) is applied to the occupied and virtual Bloch orbitals separately, yielding two independent unitary matrices, one for the occupied bands and one for the virtual bands, respectively. Hence, $\mathcal{U}(\vec{k})$ in Eq. (21) is block diagonal.

On the one hand, we want to evaluate the CO-ADC equations entirely in terms of Wannier orbitals, in the so-called Wannier or local representation;³ on the other hand, band structures are defined with respect to the crystal momentum quantum number. In what follows three different transformation schemes to switch between the local representation and the crystal momentum representation are applied to the CO-ADC formalism and their physical and methodological implications are discussed.

The dynamic self-energy $M_{nm}^\pm(\vec{k}, \omega) \equiv M_{\vec{k} \ n \ \vec{k} \ m}^\pm(\omega)$ depends on two external Bloch orbitals $\psi_{\vec{k} \ n}^\dagger(\vec{r})$ and $\psi_{\vec{k} \ m}(\vec{r})$. Hence, carrying out the inverse Wannier transformation (21b) for the external orbitals in Eq. (17) leads to

$$M_{pq}^\pm(\vec{k}, \omega) = \frac{1}{N_0} \sum_{\varrho, \sigma} \mathcal{U}_{p\varrho}(\vec{k}) \mathcal{U}_{q\sigma}^*(\vec{k}) \sum_{\vec{R}, \vec{R}'} e^{i\vec{k}\cdot(\vec{R}-\vec{R}')} M_{\vec{R} \ \varrho \ \vec{R}' \ \sigma}^\pm(\omega) \quad (22)$$

for the left-hand side of Eq. (17) and a similar expression for the right-hand side where the internal summations $\vec{l}_1, \vec{l}_2, \vec{l}_1'$, and \vec{l}_2' still run over the Brillouin zone.

In order to obtain a representation of the dynamic self-energy $M_{nm}^\pm(\vec{k}, \omega)$ entirely in terms of Wannier orbitals, it is important to note that, although matrix elements such as $U_{\vec{k} \ p; \vec{l}_1+\vec{l}_2-\vec{k} \ i \ \vec{l}_1 a \ \vec{l}_2 b}^\pm$ in Eq. (17) only depend on three independent crystal momenta, they actually describe quantities which depend on four Bloch orbitals—namely, $\psi_{\vec{k} \ p}(\vec{r})$, $\psi_{\vec{l}_1+\vec{l}_2-\vec{k} \ i}(\vec{r})$, $\psi_{\vec{l}_1 a}^\dagger(\vec{r})$, and $\psi_{\vec{l}_2 b}^\dagger(\vec{r})$ —and thus a fourfold inverse Wannier transformation (21b) has to be applied. This transformation of Eq. (17) to the Wannier representation yields

$$\begin{aligned}
M_{\vec{R}\varrho\vec{R}'\sigma}^+(\omega) &= \sum'_{\vec{g}_1\kappa, \vec{g}_2\alpha, \vec{g}_3\beta, \vec{g}'_1\kappa', \vec{g}'_2\alpha', \vec{g}'_3\beta'} \check{U}_{\vec{R}}^{\pm*} \varrho: \vec{g}_1\kappa \vec{g}_2\alpha \vec{g}_3\beta \\
&\times [\omega \mathbb{1} - \check{\mathbf{K}}^+ - \check{\mathbf{C}}^+]^{-1}_{\vec{g}_1\kappa \vec{g}_2\alpha \vec{g}_3\beta; \vec{g}'_1\kappa' \vec{g}'_2\alpha' \vec{g}'_3\beta'} \\
&\times \check{U}_{\vec{R}'\sigma; \vec{g}'_1\kappa' \vec{g}'_2\alpha' \vec{g}'_3\beta'}^+, \quad (23)
\end{aligned}$$

exploiting the unitarity of $\mathcal{U}(\vec{k})$ and the basic relations^{1,3}

$$\sum_{\vec{R}} e^{i\vec{k}\cdot\vec{R}} = N_0 \delta_{\vec{k}, \vec{0}}, \quad (24a)$$

$$\sum_{\vec{k}} e^{i\vec{k}\cdot\vec{R}} = N_0 \delta_{\vec{R}, \vec{0}}. \quad (24b)$$

The check accent on the quantities \check{U}^+ , $\check{\mathbf{K}}^+$, and $\check{\mathbf{C}}^+$ in Eq. (23) indicates that the sums run over lattice vectors and Wannier orbital indices rather than crystal momenta and band indices as in Eq. (17). The prime on the summation symbol indicates that $\vec{g}_2\alpha < \vec{g}_3\beta$ and $\vec{g}'_2\alpha' < \vec{g}'_3\beta'$ must hold to avoid double counting of contributions. The corresponding equation for $M_{\vec{R}\varrho\vec{R}'\sigma}^-(\omega)$ is formally identical to Eq. (23) apart from the changed occupation numbers $\kappa \rightarrow \alpha$, $\alpha \rightarrow \kappa$, $\beta \rightarrow \lambda$, $\kappa' \rightarrow \alpha'$, $\alpha' \rightarrow \kappa'$, and $\beta' \rightarrow \lambda'$.

One obviously Hermitian form for the dynamic self-energy emerging from Eqs. (22) and (23) is given by

$$\begin{aligned}
M_{pq}^\pm(\vec{k}, \omega) &= \sum_{\varrho, \sigma} \mathcal{U}_{p\varrho}(\vec{k}) \mathcal{U}_{q\sigma}^*(\vec{k}) \check{U}_{\varrho}^\pm(\vec{k})^\dagger \\
&\times [\omega \mathbb{1} - \check{\mathbf{K}}^\pm - \check{\mathbf{C}}^\pm]^{-1} \check{U}_{\sigma}^\pm(\vec{k}), \quad (25a)
\end{aligned}$$

$$\check{U}_{\sigma}^\pm(\vec{k}) = \frac{1}{\sqrt{N_0}} \sum_{\vec{R}} e^{i\vec{k}\cdot\vec{R}} \check{U}_{R\sigma}^\pm. \quad (25b)$$

The vector notation in Eq. (25) combines the six internal summations over the intermediate lattice vectors and Wannier orbital indices $\vec{g}_1\kappa$, $\vec{g}_2\alpha$, $\vec{g}_3\beta$, $\vec{g}'_1\kappa'$, $\vec{g}'_2\alpha'$, and $\vec{g}'_3\beta'$ in Eq. (23). We refer to Eq. (25) as the *supercell form* of CO-ADC.

The matrix $\check{\mathbf{K}}^\pm + \check{\mathbf{C}}^\pm$ in Eq. (25a) does not explicitly depend on \vec{k} which implies that its eigenvalues comprise all pole positions—i.e., pole positions for each \vec{k} point. Consequently, the resulting eigenvalues also do not explicitly depend on \vec{k} . Multiplying with $\check{U}_{\varrho}^\dagger(\vec{k})$ from the left projects on the desired set of eigenvectors. Hence, the translational symmetry among the N_0 unit cells of the crystal is not exploited to reduce the size of the configuration space which is unfavorable in conjunction with the cutoff criteria discussed in Sec. VI. In practice, Eq. (25) is applied to a molecular cluster formed by N_0 unit cells of a crystal for which Born–von Kármán boundary conditions are enforced. As a consequence, only N_0 discrete crystal momenta are in the Brillouin zone. The above given transformation from the Wannier representation to the crystal momentum representation is simple

and robust and can be used in conjunction with almost any electron correlation method, but it suffers from finite-size effects due to the, usually, small number of unit cells which are considered in practice; see, e.g., Ref. 30.

The translational symmetry of the dynamic self-energy (23) can be exploited by applying a translation by $-\vec{R}$ which removes the explicit dependence of $M_{\vec{R}\varrho\vec{R}'\sigma}^-(\omega)$ on two external lattice vectors such that it only depends on the difference of the lattice vectors according to

$$M_{\vec{R}\varrho\vec{R}'\sigma}^-(\omega) = M_{\vec{0}\varrho\vec{R}'-\vec{R}\sigma}^-(\omega) \equiv M_{\varrho\sigma}(\vec{R}' - \vec{R}, \omega). \quad (26)$$

This facilitates to remove the lattice summation over \vec{R} and the prefactor $1/N_0$ in Eq. (22) which results in (dropping the prime on \vec{R}')

$$M_{pq}^\pm(\vec{k}, \omega) = \sum_{\varrho, \sigma} \mathcal{U}_{p\varrho}(\vec{k}) \mathcal{U}_{q\sigma}^*(\vec{k}) \sum_{\vec{R}} e^{i\vec{k}\cdot\vec{R}} M_{\varrho\sigma}(\vec{R}, \omega). \quad (27)$$

To continue, we give up the idea of an ADC form for $M_{\vec{0}\varrho\vec{R}\sigma}^-(\omega)$, where the modified coupling amplitudes on the left and on the right are related by Hermitian conjugation, as is the case in Eq. (25), and arrive at

$$M_{pq}^\pm(\vec{k}, \omega) = \sum_{\varrho, \sigma} \mathcal{U}_{p\varrho}(\vec{k}) \mathcal{U}_{q\sigma}^*(\vec{k}) \check{U}_{\varrho}^{\pm\dagger} [\omega \mathbb{1} - \check{\mathbf{K}}^\pm - \check{\mathbf{C}}^\pm]^{-1} \check{U}_{\sigma}^\pm(\vec{k}), \quad (28a)$$

$$\check{U}_{\sigma}^\pm(\vec{k}) = \sum_{\vec{R}} e^{i\vec{k}\cdot\vec{R}} \check{U}_{R\sigma}^\pm, \quad (28b)$$

where a slightly changed definition of the transformed modified coupling amplitude $\check{U}_{\sigma}^\pm(\vec{k}) = \sqrt{N_0} \check{U}_{\sigma}^\pm(\vec{k})$ is employed which is indicated by a tilde accent on the quantities $\check{U}^\pm \equiv \check{U}^\pm$, $\check{\mathbf{K}}^\pm \equiv \check{\mathbf{K}}^\pm$, and $\check{\mathbf{C}}^\pm \equiv \check{\mathbf{C}}^\pm$. Because of its asymmetric nature, we denote Eq. (28) as the *semitransformed form*.

By exploiting the translational symmetry (26), we remove the summation over all translationally equivalent octuples consisting of the two external Wannier orbitals $w_{\vec{R}\varrho}^\dagger(\vec{r})$ and $w_{\vec{R}'\sigma}(\vec{r})$ of the dynamic self-energy $M_{\vec{R}\varrho\vec{R}'\sigma}^-(\omega)$ and two $2p1h$ or $2h1p$ configurations. We arrive at a summation over $\vec{R}' - \vec{R}$, ϱ , and σ in conjunction with the remaining six internal lattice vectors and Wannier orbital indices. This formulation thus provides a far better starting point for reducing the number of configurations by means of the cutoff criteria of Sec. VI than the supercell form. Using the unsymmetric ADC form (28) implies that the pole positions still do not depend explicitly on \vec{k} . Moreover, the modified coupling amplitudes (28b) are, in contrast to Eq. (25b), no longer related by Hermitian conjugation; yet, for sure, the dynamic self-energy itself stays Hermitian.

This way of exploiting translational symmetry in conjunction with the Wannier orbitals has already been applied successfully before to devise *ab initio* electron correlation methods for crystals like the local Hamiltonian approach^{32–34,36,40} or the Green's function based method of Albrecht *et al.*^{37–39}

The internal structure of the dynamic self-energy is not regarded in the two formulas (25) and (28). Expression (28) results from Eqs. (22) and (23) by exploiting the translational symmetry of $M^\pm(\vec{k}, \omega)$ in Eq. (26) and utilizing its exclusive dependence on two external Wannier orbitals. However, the translational symmetry of the matrix $\tilde{K}^\pm + \tilde{C}^\pm$ in Eq. (28) can also be exploited additionally which already was harnessed to derive Eq. (17) from its original molecular orbital formulation. We obtain

$$M_{pq}^+(\vec{k}, \omega) = \sum_{\varrho, \sigma} \mathcal{U}_{p\varrho}(\vec{k}) \mathcal{U}_{q\sigma}^*(\vec{k}) \sum_{\vec{g}_1, \vec{g}_2} \sum_{\kappa, \alpha, \beta} \bar{U}_{\varrho; \vec{g}_1 \vec{g}_2 \kappa \alpha \beta}^{+*}(\vec{k}) \times [\omega \mathbb{1} - \bar{K}^+(\vec{k}) - \bar{C}^+(\vec{k})]_{\vec{g}_1 \vec{g}_2 \kappa \alpha \beta}^{-1} \times \bar{U}_{\sigma; \vec{g}_1' \vec{g}_2' \kappa' \alpha' \beta'}^+(\vec{k}), \quad (29a)$$

$$\bar{U}_{\sigma; \vec{g}_1' \vec{g}_2' \kappa' \alpha' \beta'}^+(\vec{k}) = \sum_{\vec{R}} e^{i\vec{k} \cdot \vec{R}} \bar{U}_{R\sigma; 0\kappa' \vec{g}_1' \vec{g}_2' \beta'}^+, \quad (29b)$$

$$[\bar{K}^+(\vec{k}) + \bar{C}^+(\vec{k})]_{\vec{g}_1' \vec{g}_2' \kappa' \alpha' \beta'}^{\vec{g}_1 \vec{g}_2 \kappa \alpha \beta} = \sum_{\vec{R}} e^{i\vec{k} \cdot \vec{R}} (\bar{K}^+ + \bar{C}^+)_{R\kappa' \vec{g}_1' + \vec{R} \alpha' \vec{g}_2' + \vec{R} \beta'}^{\vec{g}_1 \vec{g}_2 \kappa \alpha \beta}, \quad (29c)$$

where the identities $\bar{U}^+ \equiv \check{U}^+$, $\bar{K}^+ \equiv \check{K}^+$, and $\bar{C}^+ \equiv \check{C}^+$ hold. The corresponding relations for $M^-(\vec{k}, \omega)$ are formally identical to Eq. (29) apart from the changed occupation numbers $\kappa \rightarrow \alpha$, $\alpha \rightarrow \kappa$, $\beta \rightarrow \lambda$, $\kappa' \rightarrow \alpha'$, $\alpha' \rightarrow \kappa'$, and $\beta' \rightarrow \lambda'$. Alternatively, we can derive Eq. (29) by inserting the inverse Wannier transformation (21b) into the CO-ADC equations for Bloch orbitals (17) which already are fully adapted to translational symmetry. We refer to Eq. (29) as the *fully translational symmetry-adapted form*.

The modified coupling amplitudes (29b) are constructed by considering only Wannier orbitals relative to an origin cell (or reference cell) where the hole with index κ is assumed to reside. The external orbital index σ of a modified coupling amplitude can be viewed to represent a Bloch orbital $\psi_{\vec{k}\sigma}(\vec{r})$. This orbital interacts with the $2p1h$ configurations that are pinned with one lattice vector to the origin cell and extend with the two remaining lattice vectors \vec{g}_1 and \vec{g}_2 over up to two different unit cells. Alternatively, one can use the translational symmetry of the $\bar{U}_{R\sigma; 0\kappa' \vec{g}_1' \vec{g}_2' \beta'}^+$ to arrive at

$$\bar{U}_{\sigma; \vec{g}_1' \vec{g}_2' \kappa' \alpha' \beta'}^+(\vec{k}) = \sum_{\vec{R}} e^{-i\vec{k} \cdot \vec{R}} \bar{U}_{0\sigma; R\kappa' \vec{g}_1' + \vec{R} \alpha' \vec{g}_2' + \vec{R} \beta'}^+. \quad (30)$$

Now the external orbital is $w_{0\sigma}(\vec{r})$ which is independent of \vec{R} and consequently Eq. (30) is interpreted to describe the interaction of a Wannier orbital in the origin cell with $2p1h$ configurations centered around all lattice vectors \vec{R} which are combined to give an intermediate $2p1h$ configuration with a total crystal momentum $-\vec{k}$.

The matrix $\bar{K}^+ + \bar{C}^+$ in Eq. (29c) describes the coupling among the $2p1h$ configurations. One of the lattice vectors of

the first triple of Wannier orbitals is pinned to the origin cell, and the two other lattice vectors \vec{g}_1 and \vec{g}_2 are offsets to it. The remaining three lattice vectors belong to a Wannier orbital in an arbitrary cell \vec{R} and two further Wannier orbitals in the cells $\vec{g}_1 + \vec{R}$ and $\vec{g}_2 + \vec{R}$ relative to the former. Obviously the entire Eq. (29c) can be interpreted to describe the interaction of a $2p1h$ configuration of Wannier orbitals centered around the origin cell with another $2p1h$ configuration with crystal momentum \vec{k} . Due to the full exploitation of translational symmetry, also of the intermediate $2p1h$ configurations, the fully translational symmetry adapted form yields the smallest configuration space in conjunction with the cut-off criteria of Sec. VI.

In order to give explicit CO-ADC expressions for the matrices showing up in Eq. (29), we transform the Hamiltonian (2) with the help of formula (21b) to the Wannier representation. A similar decomposition as in Eq. (2) is chosen for a subsequent application of perturbation theory:

$$\hat{H} = \hat{H}_0^{\text{WF}} + \hat{H}_1^{\text{WF}},$$

$$\hat{H}_0^{\text{WF}} = \sum_{\vec{R}\varrho} \varepsilon_{\vec{R}\varrho} \hat{c}_{\vec{R}\varrho}^\dagger \hat{c}_{\vec{R}\varrho},$$

$$\hat{H}_1^{\text{WF}} = \sum_{\vec{R}_1\varrho, \vec{R}_2\sigma} W_{\vec{R}_1\varrho, \vec{R}_2\sigma} \hat{c}_{\vec{R}_1\varrho}^\dagger \hat{c}_{\vec{R}_2\sigma} + \frac{1}{2} \sum_{\substack{\vec{R}_1\varrho, \vec{R}_2\sigma, \\ \vec{R}_3\tau, \vec{R}_4\nu}} V_{\vec{R}_1\varrho, \vec{R}_2\sigma, \vec{R}_3\tau, \vec{R}_4\nu} \times \hat{c}_{\vec{R}_1\varrho}^\dagger \hat{c}_{\vec{R}_2\sigma}^\dagger \hat{c}_{\vec{R}_4\nu} \hat{c}_{\vec{R}_3\tau}, \quad (31)$$

with $\varepsilon_{\vec{R}\varrho} \equiv F_{\vec{R}\varrho, \vec{R}\varrho} = F_{0\varrho, 0\varrho}$ being the diagonal elements of the Fock matrix \mathbf{F} . Here $W_{\vec{R}_1\varrho, \vec{R}_2\sigma} = -\sum_{\vec{R}\tau} V_{\vec{R}_1\varrho, \vec{R}\tau} V_{\vec{R}\tau, \vec{R}_2\sigma} + (1 - \delta_{\vec{R}_1\varrho, \vec{R}_2\sigma}) F_{\vec{R}_1\varrho, \vec{R}_2\sigma}$ comprises the negative of the Hartree-Fock potential and also the off-diagonal elements of the Fock matrix. Note that \mathbf{F} is block diagonal and thus the Wannier orbitals are still separated into occupied and virtual Wannier orbitals.

Using the inverse generalized Wannier transformation (21b)—as is done throughout this article—corresponds to the use of the full Fock matrix as zeroth-order Hamiltonian. In addition, a perturbative expansion of the off-diagonal elements in the Fock matrix is applied in succession of the inverse Wannier transformation. This conduct is equivalent to employing the partitioning of the Fock matrix introduced in Eq. (31).

The one-electron interaction is mediated by the off-diagonal Fock matrix elements, and the two-electron interaction is represented by the two-electron integrals; let the one-electron interaction be treated using Feynman diagrams up to m th order and account for diagrams which exclusively involve two-electron interactions of highest order n . This separation facilitates to take higher-order terms into account for the slow convergent series; the resulting scheme is denoted by CO-ADC(m, n).

The CO-ADC(2,2) approximation for Wannier orbitals is obtained similarly to the case of the CO-ADC(2) approximation for Bloch orbitals (18) and reads

$$\bar{U}_{RQ\bar{g}_1\kappa\bar{g}_2\alpha\bar{g}_3\beta}^+ = V_{RQ\bar{g}_1\kappa[\bar{g}_2\alpha\bar{g}_3\beta]}^* n_{\bar{g}_1\kappa} \bar{n}_{\bar{g}_2\alpha} \bar{n}_{\bar{g}_3\beta}, \quad (32a)$$

$$\bar{K}_{\bar{g}_1\kappa\bar{g}_2\alpha\bar{g}_3\beta}^+ = \delta_{\bar{g}_1\kappa\bar{g}_2\alpha\bar{g}_3\beta; \bar{g}'_1\kappa'\bar{g}'_2\alpha'\bar{g}'_3\beta'} (\varepsilon_{\bar{g}_2\alpha} + \varepsilon_{\bar{g}_3\beta} - \varepsilon_{\bar{g}_1\kappa}) n_{\bar{g}_1\kappa} \bar{n}_{\bar{g}_2\alpha} \bar{n}_{\bar{g}_3\beta}, \quad (32b)$$

$$\bar{C}_{\bar{g}_1\kappa\bar{g}_2\alpha\bar{g}_3\beta}^+ = 0. \quad (32c)$$

The equations for \bar{U}^- , \bar{K}^- , and \bar{C}^- are formally identical to Eq. (32) upon modifying the labels according to the adaptation of Eq. (29) to $M_{pq}^-(\vec{k}, \omega)$ and replacing the occupation numbers in Eqs. (32a) and (32b) by $\bar{n}_{\bar{g}_1\kappa} n_{\bar{g}_2\alpha} n_{\bar{g}_3\beta}$. Up to second order, the perturbative treatment of the off-diagonal elements of the Fock matrix does not introduce any new diagrams for the dynamic self-energy and thus $\bar{K}^\pm + \bar{C}^\pm$ remains diagonal.^{50,61} However, in a formulation which is invariant under unitary transformations in the occupied and virtual space, this is no longer the case because the full Fock matrix needs to be chosen as the zeroth-order Hamiltonian in place of \hat{H}_0^{WF} then.^{41,93}

IV. STATIC SELF-ENERGY

A. Crystal momentum representation

The static self-energy has not been determined so far. It is represented by all those diagrams in the diagrammatic expansion of the self-energy where the external points of the diagrams correspond to equal times.⁵⁰ In a strict second-order treatment of electron correlations, using Bloch orbitals (2), the static self-energy is zero because the first static self-energy diagrams arise the earliest in third order. Moreover, it turns out that the diagrammatic series for the static self-energy does not converge reasonably in many cases.⁶⁰ However, a self-consistent solution is possible^{51,55} utilizing^{50,87,88}

$$\Sigma_{pq}^\infty(\vec{k}) = W_{pq}(\vec{k}) + \sum_{\vec{k}'} \sum_{r,s} V_{\vec{k}p\vec{k}'r[\vec{k}q\vec{k}'s]} V_{\vec{k}p\vec{k}'r[\vec{k}q\vec{k}'s]} \times \left[\frac{1}{2\pi i} \oint G_{sr}(\vec{k}', \omega) d\omega \right], \quad (33)$$

here given in terms of Bloch orbitals. The contour integration in Eq. (33) runs along the real axis and closes in the upper complex ω plane, hence enclosing only the poles of the advanced Green's function $G^-(\vec{k}', \omega)$ in Eq. (6b).

The self-consistent solution of Eq. (33) is computationally expensive. Yet a stable and efficient Dyson expansion method (DEM) for determining the static self-energy is devised in Ref. 60. There, the first two terms of the Dyson expansion (9b) are inserted into Eq. (33). The term $W_{pq}(\vec{k})$ in Eq. (33) cancels the result of the contour integration over the free Green's function $G_{sr}^0(\vec{k}', \omega)$. Carrying out the contour integration over the product of the two free Green's functions and the static self-energy yields

$$\Sigma_{pq}^\infty(\vec{k}) = \sum_{\vec{k}'} \sum_{r,s} A_{\vec{k}p\vec{k}'r[\vec{k}q\vec{k}'s]} \Sigma_{sr}^\infty(\vec{k}') + b_{pq}(\vec{k}), \quad (34a)$$

$$A_{\vec{k}p\vec{k}'r[\vec{k}q\vec{k}'s]} = V_{\vec{k}p\vec{k}'r[\vec{k}q\vec{k}'s]} (\varepsilon_{\vec{k}'r} - \varepsilon_{\vec{k}'s})^{-1} [n_{\vec{k}'r} \bar{n}_{\vec{k}'s} - \bar{n}_{\vec{k}'r} n_{\vec{k}'s}], \quad (34b)$$

$$b_{pq}(\vec{k}) = \sum_{\vec{k}'} \sum_{r,s} V_{\vec{k}p\vec{k}'r[\vec{k}q\vec{k}'s]} Q_{rs}(\vec{k}'), \quad (34c)$$

$$Q_{rs}(\vec{k}') = \frac{1}{2\pi i} \oint G_{ss}^0(\vec{k}', \omega) M_{sr}(\vec{k}', \omega) G_{rr}^0(\vec{k}', \omega) d\omega. \quad (34d)$$

The $Q_{sr}(\vec{k}')$ can now be determined by inserting the spectral representation of the dynamic self-energy (13) into Eq. (34d). Carrying out the contour integration yields

$$Q_{rs}(\vec{k}') = Q_{rs}^+(\vec{k}') + Q_{rs}^-(\vec{k}'), \quad (35a)$$

$$Q_{rs}^+(\vec{k}') = \sum_{n \in \{N+1\}} m_s^{+, (n)}(\vec{k}') m_r^{+, (n)*}(\vec{k}') \times \left[\frac{-n_{\vec{k}'r} \bar{n}_{\vec{k}'s}}{[\varepsilon_{\vec{k}'r} - \omega_n^+(\vec{k}')][\varepsilon_{\vec{k}'s} - \omega_n^+(\vec{k}')]} + \frac{n_{\vec{k}'r} \bar{n}_{\vec{k}'s}}{(\varepsilon_{\vec{k}'r} - \varepsilon_{\vec{k}'s})[\varepsilon_{\vec{k}'r} - \omega_n^+(\vec{k}')]} - \frac{\bar{n}_{\vec{k}'r} n_{\vec{k}'s}}{(\varepsilon_{\vec{k}'r} - \varepsilon_{\vec{k}'s})[\varepsilon_{\vec{k}'s} - \omega_n^+(\vec{k}')]} \right], \quad (35b)$$

$$Q_{rs}^-(\vec{k}') = \sum_{n \in \{N-1\}} m_s^{-, (n)}(\vec{k}') m_r^{-, (n)*}(\vec{k}') \times \left[\frac{\bar{n}_{\vec{k}'r} n_{\vec{k}'s}}{[\varepsilon_{\vec{k}'r} - \omega_n^-(\vec{k}')][\varepsilon_{\vec{k}'s} - \omega_n^-(\vec{k}')]} - \frac{\bar{n}_{\vec{k}'r} n_{\vec{k}'s}}{(\varepsilon_{\vec{k}'r} - \varepsilon_{\vec{k}'s})[\varepsilon_{\vec{k}'r} - \omega_n^-(\vec{k}')]} + \frac{n_{\vec{k}'r} \bar{n}_{\vec{k}'s}}{(\varepsilon_{\vec{k}'r} - \varepsilon_{\vec{k}'s})[\varepsilon_{\vec{k}'s} - \omega_n^-(\vec{k}')]} \right]. \quad (35c)$$

In order to evaluate Eq. (35), from now on, we resort to the ADC form of the dynamic self-energy in terms of Bloch orbitals (17). By affixing a bar accent to the quantities $U^\pm(\vec{k})$, $K^\pm(\vec{k})$, and $C^\pm(\vec{k})$ in all following equations of this subsection, they become formally identical to the ones obtained with the fully translational symmetry-adapted form (29).

The direct usage of Eq. (35) is in practice very time consuming because the $K^\pm(\vec{k}') + C^\pm(\vec{k}')$ matrix has to be diagonalized fully (19) to obtain the pole positions $\omega_n^\pm(\vec{k}')$ of the spectral representation (13). For the CO-ADC(2) approximation of the dynamic self-energy in crystal momentum repre-

sentation (18), however, $\mathbf{K}^\pm(\vec{k}') + \mathbf{C}^\pm(\vec{k}')$ remains diagonal. This leads to $m_r^{\pm(n)*}(\vec{k}') = U_{\vec{k}',r,n}^\pm$ and $\omega_n^\pm(\vec{k}') = K_{nn}^\pm(\vec{k}')$ where the n th eigenvector of $\mathbf{K}^\pm(\vec{k}') + \mathbf{C}^\pm(\vec{k}')$ is unity for a single $2p1h$ or $2h1p$ configuration, respectively, and zero otherwise. In general, the $Q_{rs}(\vec{k}')$ are determined efficiently from Eq. (35) by the inversion method or by a single-vector Lanczos diagonalization to circumvent a full diagonalization of $\mathbf{K}^\pm(\vec{k}') + \mathbf{C}^\pm(\vec{k}')$.⁶⁰

The inversion method has been found to be more efficient⁶⁰ than the single-vector Lanczos diagonalization, so we concentrate on the former. We define auxiliary vectors $\vec{V}_r^\pm(\vec{k}')$ as the solution of the inhomogeneous systems of linear equations

$$[\varepsilon_{\vec{k}',r} - \mathbf{K}^\pm(\vec{k}') - \mathbf{C}^\pm(\vec{k}')] \vec{V}_r^\pm(\vec{k}') = \vec{U}_r^\pm(\vec{k}'). \quad (36)$$

Inserting the eigenvector matrix $\mathbf{Y}^\pm(\vec{k}')$ from Eq. (19) into Eq. (36), one obtains, by using formula (20),

$$\vec{V}_r^\pm(\vec{k}') = \mathbf{Y}^\pm(\vec{k}') [\varepsilon_{\vec{k}',r} - \mathbf{\Omega}^\pm(\vec{k}')]^{-1} \vec{m}_r^{\pm\dagger}(\vec{k}'), \quad (37)$$

which reveals the usefulness of the new vectors and allows us to rewrite Eq. (35) as follows:

$$\begin{aligned} Q_{rs}^+(\vec{k}') = & -\vec{V}_s^{+\dagger}(\vec{k}') \vec{V}_r^+(\vec{k}') n_{\vec{k}',r} n_{\vec{k}',s} + (\varepsilon_{\vec{k}',r} - \varepsilon_{\vec{k}',s})^{-1} \\ & \times [\vec{U}_s^{+\dagger}(\vec{k}') \vec{V}_r^+(\vec{k}') n_{\vec{k}',r} n_{\vec{k}',s} - \vec{V}_s^{+\dagger}(\vec{k}') \vec{U}_r^+(\vec{k}') n_{\vec{k}',r} n_{\vec{k}',s}], \end{aligned} \quad (38a)$$

$$\begin{aligned} Q_{rs}^-(\vec{k}') = & \vec{V}_s^{-\dagger}(\vec{k}') \vec{V}_r^-(\vec{k}') n_{\vec{k}',r} n_{\vec{k}',s} - (\varepsilon_{\vec{k}',r} - \varepsilon_{\vec{k}',s})^{-1} \\ & \times [\vec{U}_s^{-\dagger}(\vec{k}') \vec{V}_r^-(\vec{k}') n_{\vec{k}',r} n_{\vec{k}',s} - \vec{V}_s^{-\dagger}(\vec{k}') \vec{U}_r^-(\vec{k}') n_{\vec{k}',r} n_{\vec{k}',s}]. \end{aligned} \quad (38b)$$

We have reduced the problem of determining the $Q_{rs}^\pm(\vec{k}')$ to the problem of determining the $\vec{V}_r^\pm(\vec{k}')$. Inspecting Eqs. (36) and (38), we note that we have to solve for the $\vec{V}_r^\pm(\vec{k}')$ in the large $2p1h$ -configuration space but only for the usually small set of all occupied orbitals. Conversely, the $\vec{V}_r^\pm(\vec{k}')$ have to be calculated in the small $2h1p$ -configuration space but for the usually large set of all virtual orbitals.

The diagonal parts $\varepsilon_{\vec{k}',r} - \mathbf{K}^\pm(\vec{k}')$ in Eq. (36) are, at least, of a magnitude of twice the Hartree-Fock band gap, implying usually a diagonal dominance of the full matrices in Eq. (36). Therefore, a solution by Jacobi iterations^{60,94} is suggested:

$$\vec{V}_r^{\pm(0)}(\vec{k}') = [\varepsilon_{\vec{k}',r} - \mathbf{K}^\pm(\vec{k}')]^{-1} \vec{U}_r^\pm(\vec{k}'),$$

$$\vec{V}_r^{\pm(n)}(\vec{k}') = \vec{V}_r^{\pm(0)}(\vec{k}') + [\varepsilon_{\vec{k}',r} - \mathbf{K}^\pm(\vec{k}')]^{-1} \mathbf{C}^\pm(\vec{k}') \vec{V}_r^{\pm(n-1)}(\vec{k}'), \quad (39)$$

which turns out to converge rapidly.

The inhomogeneous linear system of equations (34a) can now be solved for $\Sigma_{pq}^\infty(\vec{k})$ by a matrix inversion.⁵¹

$$\vec{\Sigma}^\infty = (1 - \mathbf{A})^{-1} \vec{b}, \quad (40)$$

where Σ_i^∞ , b_i , and A_{ij} are composed by numerating the compound indices (p, q, \vec{k}) and (s, r, \vec{k}') in $\Sigma_{pq}^\infty(\vec{k})$, $b_{pq}^\infty(\vec{k})$, and $A_{\vec{k}p\vec{k}q, \vec{k}'s\vec{k}'r}$ by integer numbers i and j , respectively. Inspecting Eq. (34b), we note that \mathbf{A} couples only to the components of $\Sigma_{sr}^\infty(\vec{k}')$ where the s, r indices denote a combination of particle-hole or hole-particle orbitals. As all quantities in Eq. (40) are Hermitian, we can further restrict the band indices to $p \leq q$. As soon as the number of \vec{k} points becomes large, the solution of Eq. (40) gets cumbersome as the dimension of the system of linear equations is given by the number of entries of the upper triangle (including the diagonal entries) of the static self-energy matrix times the number of \vec{k} points. Thus an iterative linear equations solver has to be employed.⁹⁴

B. Wannier representation

The static self-energy can also be determined directly in Wannier representation. Having expressed the static self-energy in terms of Wannier orbitals, we obtain the static self-energy in crystal momentum representation by

$$\Sigma_{pq}^\infty(\vec{k}) = \sum_{\varrho, \sigma} \mathcal{U}_{p\varrho}(\vec{k}) \mathcal{U}_{q\sigma}^*(\vec{k}) \sum_{\vec{R}} e^{i\vec{k}\cdot\vec{R}} \Sigma_{\varrho\sigma}^\infty(\vec{R}). \quad (41)$$

To find an approximation for $\Sigma_{\varrho\sigma}^\infty(\vec{R})$, we insert the inverse Wannier transformation (21b) and its Hermitian conjugate into Eq. (34) and arrive at

$$\Sigma_{\varrho\sigma}^\infty(\vec{R}) = \sum_{\vec{R}'} \sum_{\tau, \nu} \left[\sum_{\vec{g}} A_{0\varrho\vec{R}\sigma, \vec{g}\nu\vec{g}+\vec{R}'} \Sigma_{\nu\tau}^\infty(\vec{R}') + b_{\varrho\sigma}(\vec{R}), \right] \quad (42a)$$

$$b_{\varrho\sigma}(\vec{R}) = \sum_{\vec{R}'} \sum_{\tau, \nu} \left[\sum_{\vec{g}} V_{0\varrho\vec{g}+\vec{R}'\tau, \vec{R}\sigma\vec{g}\nu} \right] Q_{\tau\nu}(\vec{R}'). \quad (42b)$$

Note that the translational symmetry of $A_{0\varrho\vec{R}\sigma, \vec{g}\nu\vec{g}+\vec{R}'\tau}$ could only be utilized once to remove one lattice summation such that two lattice summations (one over \vec{R}' and one over \vec{g}) show up in Eq. (42) while only one summation over \vec{k}' is necessary in Eq. (34). There is no first-order contribution to the static self-energy in Eq. (42) because the static self-energy used here evolves from an inverse Wannier transformation of the self-energy obtained in Møller-Plesset partition⁷⁷⁻⁷⁹ and a subsequent perturbative expansion with respect to the off-diagonal elements of the Fock matrix.

For the remaining Eqs. (34b) and (34d), we assume the partition (31) of the Hamiltonian in Wannier representation, to obtain

$$\begin{aligned} A_{0\varrho\vec{R}\sigma, \vec{g}\nu\vec{g}+\vec{R}'\tau} = & V_{0\varrho\vec{g}+\vec{R}'\tau, \vec{R}\sigma\vec{g}\nu} (\varepsilon_{\vec{g}+\vec{R}'\tau} - \varepsilon_{\vec{g}\nu})^{-1} \\ & \times (n_{\vec{g}+\vec{R}'\tau} n_{\vec{g}\nu} - n_{\vec{g}+\vec{R}'\tau} n_{\vec{g}\nu}), \end{aligned} \quad (43a)$$

$$Q_{\tau\nu}(\vec{R}') \equiv Q_{\vec{R}'\tau\vec{0}\nu} = \frac{1}{2\pi i} \oint G_{\nu\nu}^0(\vec{0}, \omega) \times M_{\nu\tau}(\vec{R}', \omega) G_{\tau\tau}^0(\vec{0}, \omega) d\omega, \quad (43b)$$

with the free Green's function in Wannier representation given by

$$G_{\tau\nu}^0(\vec{R}' - \vec{R}, \omega) \equiv G_{\vec{R}\tau\vec{R}'\nu}^0(\omega) = \delta_{\vec{R}\tau, \vec{R}'\nu} \left[\frac{\bar{n}_{\vec{R}\tau}}{\omega - \varepsilon_{\vec{R}\tau} + i\eta} + \frac{n_{\vec{R}\tau}}{\omega - \varepsilon_{\vec{R}\tau} - i\eta} \right]. \quad (44)$$

To determine the $Q_{\tau\nu}(\vec{R}')$, we introduce the spectral representation of the dynamic self-energy in Wannier representation [the analog of Eq. (13)]:

$$M_{\nu\tau}(\vec{R}', \omega) = \sum_{n \in \{N+1\}} \frac{\check{m}_\nu^{+, (n)}(\vec{0}) \check{m}_\tau^{+, (n)*}(\vec{R}')}{\omega - \check{\omega}_n^+ + i\eta} + \sum_{n \in \{N-1\}} \frac{\check{m}_\nu^{-, (n)}(\vec{0}) \check{m}_\tau^{-, (n)*}(\vec{R}')}{\omega - \check{\omega}_n^- - i\eta} = M_{\nu\tau}^+(\vec{R}', \omega) + M_{\nu\tau}^-(\vec{R}', \omega), \quad (45)$$

which is obtained from the ADC form of the dynamic self-energy in Wannier representation (23) by letting $\vec{R} \rightarrow \vec{0}$ and diagonalizing $\check{\mathbf{K}}^\pm + \check{\mathbf{C}}^\pm$ analogously to Eq. (19). Since translational symmetry cannot be exploited in Eq. (23) as \vec{R}' —in contrast to \vec{k} —is not a good quantum number; this leads to the redundancies that have already been mentioned in conjunction with the supercell form of the dynamic self-energy in Eq. (25); namely, the full configuration space of $2p1h$ and $2h1p$ configurations from the N_0 unit cells of the crystal is necessary here. However, the cutoff criterion of Sec. VI, nevertheless, can be applied.

The $Q_{\tau\nu}(\vec{R}')$ can now be determined by inserting Eq. (45) into Eq. (43b). Carrying out the contour integration yields

$$Q_{\tau\nu}(\vec{R}') = Q_{\tau\nu}^+(\vec{R}') + Q_{\tau\nu}^-(\vec{R}'), \quad (46a)$$

$$Q_{\tau\nu}^+(\vec{R}') = \sum_{n \in \{N+1\}} \check{m}_\nu^{+, (n)}(\vec{0}) \check{m}_\tau^{+, (n)*}(\vec{R}') \times \left[\frac{-n_{\vec{R}'\tau} n_{\vec{0}\nu}}{[\varepsilon_{\vec{R}'\tau} - \check{\omega}_n^+][\varepsilon_{\vec{0}\nu} - \check{\omega}_n^+]} + \frac{n_{\vec{R}'\tau} \bar{n}_{\vec{0}\nu}}{(\varepsilon_{\vec{R}'\tau} - \varepsilon_{\vec{0}\nu})[\varepsilon_{\vec{R}'\tau} - \check{\omega}_n^+]} - \frac{\bar{n}_{\vec{R}'\tau} n_{\vec{0}\nu}}{(\varepsilon_{\vec{R}'\tau} - \varepsilon_{\vec{0}\nu})[\varepsilon_{\vec{0}\nu} - \check{\omega}_n^+]} \right], \quad (46b)$$

$$Q_{\tau\nu}^-(\vec{R}') = \sum_{n \in \{N-1\}} \check{m}_\nu^{-, (n)}(\vec{0}) \check{m}_\tau^{-, (n)*}(\vec{R}') \times \left[\frac{\bar{n}_{\vec{R}'\tau} \bar{n}_{\vec{0}\nu}}{[\varepsilon_{\vec{R}'\tau} - \check{\omega}_n^-][\varepsilon_{\vec{0}\nu} - \check{\omega}_n^-]} - \frac{\bar{n}_{\vec{R}'\tau} n_{\vec{0}\nu}}{(\varepsilon_{\vec{R}'\tau} - \varepsilon_{\vec{0}\nu})[\varepsilon_{\vec{R}'\tau} - \check{\omega}_n^-]} + \frac{n_{\vec{R}'\tau} \bar{n}_{\vec{0}\nu}}{(\varepsilon_{\vec{R}'\tau} - \varepsilon_{\vec{0}\nu})[\varepsilon_{\vec{0}\nu} - \check{\omega}_n^-]} \right]. \quad (46c)$$

We proceed as before by defining the auxiliary vectors

$$[\varepsilon_{\vec{R}'\varrho} 1 - \check{\mathbf{K}}^\pm - \check{\mathbf{C}}^\pm] \vec{V}_\varrho^\pm(\vec{R}') = \vec{U}_\varrho^\pm(\vec{R}'), \quad (47)$$

setting $\vec{U}_\varrho^\pm(\vec{R}) \equiv \vec{U}_{\vec{R}\varrho}^\pm$, and rewrite Eq. (46):

$$Q_{\tau\nu}^+(\vec{R}') = -\vec{V}_\nu^{+\dagger}(\vec{0}) \vec{V}_\tau^+(\vec{R}') n_{\vec{R}'\tau} n_{\vec{0}\nu} + (\varepsilon_{\vec{R}'\tau} - \varepsilon_{\vec{0}\nu})^{-1} \times [\vec{U}_\nu^{+\dagger}(\vec{0}) \vec{V}_\tau^+(\vec{R}') n_{\vec{R}'\tau} \bar{n}_{\vec{0}\nu} - \vec{V}_\nu^{+\dagger}(\vec{0}) \vec{U}_\tau^+(\vec{R}') \bar{n}_{\vec{R}'\tau} n_{\vec{0}\nu}], \quad (48a)$$

$$Q_{\tau\nu}^-(\vec{R}') = \vec{V}_\nu^{-\dagger}(\vec{0}) \vec{V}_\tau^-(\vec{R}') \bar{n}_{\vec{R}'\tau} \bar{n}_{\vec{0}\nu} - (\varepsilon_{\vec{R}'\tau} - \varepsilon_{\vec{0}\nu})^{-1} \times [\vec{U}_\nu^{-\dagger}(\vec{0}) \vec{V}_\tau^-(\vec{R}') \bar{n}_{\vec{R}'\tau} n_{\vec{0}\nu} - \vec{V}_\nu^{-\dagger}(\vec{0}) \vec{U}_\tau^-(\vec{R}') n_{\vec{R}'\tau} \bar{n}_{\vec{0}\nu}]. \quad (48b)$$

The algorithm for Jacobi iterations now reads

$$\vec{V}_\varrho^{\pm, (0)}(\vec{R}') = [\varepsilon_{\vec{R}'\varrho} 1 - \check{\mathbf{K}}^\pm]^{-1} \vec{U}_\varrho^\pm(\vec{R}'),$$

$$\vec{V}_\varrho^{\pm, (n)}(\vec{R}') = \vec{V}_\varrho^{\pm, (0)}(\vec{R}') + [\varepsilon_{\vec{R}'\varrho} 1 - \check{\mathbf{K}}^\pm]^{-1} \check{\mathbf{C}}^\pm \vec{V}_\varrho^{\pm, (n-1)}(\vec{R}'), \quad (49)$$

and the inhomogeneous linear system of equations (42a) can be solved for $\check{\Sigma}_{\varrho\sigma}^\infty(\vec{R})$ by a matrix inversion:⁵¹

$$\check{\Sigma}^\infty = (1 - \check{\mathbf{A}})^{-1} \check{\mathbf{b}}, \quad (50)$$

where a check accent is affixed to indicate that Wannier orbitals rather than Bloch orbitals are used. We employ a mapping of the compound indices $(\varrho, \sigma, \vec{R})$ and (ν, τ, \vec{R}') to the integer numbers i and j , respectively, for the quantities $\check{\Sigma}_i^\infty$, \check{b}_i , and \check{A}_{ij} . Note that $\check{\Sigma}^\infty(\vec{R})$ is not Hermitian. Hence, the full static self-energy matrix has to be included in $\check{\Sigma}^\infty$ explicitly for several lattice vectors \vec{R} . However, the property $\check{\Sigma}^{\infty\dagger}(\vec{R}) = \check{\Sigma}^\infty(-\vec{R})$ holds which can be utilized to reduce the number of equations in formula (50). Nevertheless, in many cases, the linear system of equations needs to be solved iteratively.⁹⁴

V. DYSON EQUATION

Having determined approximations for the static and the dynamic self-energy in terms of Wannier orbitals in Eqs. (41) and (29), respectively, we can finally determine the positions and strengths of the poles of the one-particle Green's function from Eq. (10). [The pole positions and strengths of the

Green's function, using Bloch orbitals to represent the self-energy (34) and (17), can be obtained following a nearly identical line of argument.] To this end, the small Hermitian eigenvalue problem

$$[\boldsymbol{\varepsilon}(\vec{k}) + \bar{\boldsymbol{\Sigma}}^\infty(\vec{k}) + \bar{\mathbf{M}}(\vec{k}, \omega)]\vec{x}_G(\vec{k}, \omega) = \omega\vec{x}_G(\vec{k}, \omega), \quad (51)$$

with $\boldsymbol{\varepsilon}(\vec{k})$ being the diagonal matrix of Bloch orbital energies and $\vec{x}_G(\vec{k}, \omega)$ denoting eigenvectors, has to be solved self-consistently—i.e., such that the energy ω entering the dynamic self-energy $\bar{\mathbf{M}}(\vec{k}, \omega)$ is identical to the resulting eigenvalue ω .

To avoid the unitary matrices $\mathcal{U}(\vec{k})$ and $\mathcal{U}^\dagger(\vec{k})$ in Eqs. (29a) and (41) arising in the following expressions, we multiply Eq. (51) from the left with $\mathcal{U}^\dagger(\vec{k})$ and insert $\mathcal{U}(\vec{k})\mathcal{U}^\dagger(\vec{k})=1$ between the right parenthesis and the eigenvector \vec{x}_G on the left-hand side of the formula. Defining the translational symmetry-adapted Fock matrix $\bar{F}_{\rho\sigma}(\vec{k})=\sum_{\vec{R}}e^{i\vec{k}\cdot\vec{R}}F_{\rho\sigma}(\vec{R})$, one arrives at

$$[\bar{F}(\vec{k}) + \bar{\boldsymbol{\Sigma}}^\infty(\vec{k}) + \bar{\mathbf{M}}(\vec{k}, \omega)]\vec{x}_G(\vec{k}, \omega) = \omega\vec{x}_G(\vec{k}, \omega), \quad (52)$$

where the new quantities $\bar{F}_{\rho\sigma}(\vec{k})$, $\bar{\boldsymbol{\Sigma}}^\infty_{\rho\sigma}(\vec{k})$, $\bar{M}_{\rho\sigma}(\vec{k}, \omega)$, and $x_{G,\rho}(\vec{k}, \omega)$ are related to the old ones $\varepsilon_{pq}(\vec{k})$, $\Sigma_{pq}^\infty(\vec{k})$, $M_{pq}(\vec{k}, \omega)$, and $x_{G,p}(\vec{k}, \omega)$ by $\boldsymbol{\varepsilon}(\vec{k})=\mathcal{U}(\vec{k})\bar{F}(\vec{k})\mathcal{U}^\dagger(\vec{k})$, $\bar{\boldsymbol{\Sigma}}^\infty(\vec{k})=\mathcal{U}(\vec{k})\boldsymbol{\Sigma}^\infty(\vec{k})\mathcal{U}^\dagger(\vec{k})$, $\bar{\mathbf{M}}(\vec{k}, \omega)=\mathcal{U}(\vec{k})\mathbf{M}(\vec{k}, \omega)\mathcal{U}^\dagger(\vec{k})$, and $\vec{x}_G(\vec{k}, \omega)=\mathcal{U}(\vec{k})\vec{x}_G(\vec{k}, \omega)$.

Inserting the ADC form of the dynamic self-energy (29a) into Eq. (52) and defining

$$\bar{x}^\pm(\vec{k}, \omega) = [\omega 1 - \bar{\mathbf{K}}^\pm(\vec{k}) - \bar{\mathbf{C}}^\pm(\vec{k})]^{-1}\bar{\mathbf{U}}^\pm(\vec{k})\vec{x}_G(\vec{k}, \omega) \quad (53)$$

yields the following form of the eigenvalue problem (52):

$$\begin{aligned} &(\bar{F}(\vec{k}) + \bar{\boldsymbol{\Sigma}}^\infty(\vec{k}))\vec{x}_G(\vec{k}, \omega) + \bar{\mathbf{U}}^{+\dagger}(\vec{k})\bar{x}^+(\vec{k}, \omega) + \bar{\mathbf{U}}^{-\dagger}(\vec{k})\bar{x}^-(\vec{k}, \omega) \\ &= \omega\vec{x}_G(\vec{k}, \omega). \end{aligned} \quad (54)$$

Rewriting Eq. (53) as

$$\bar{\mathbf{U}}^\pm(\vec{k})\vec{x}_G(\vec{k}, \omega) + (\bar{\mathbf{K}}^\pm(\vec{k}) + \bar{\mathbf{C}}^\pm(\vec{k}))\bar{x}^\pm(\vec{k}, \omega) = \omega\bar{x}^\pm(\vec{k}, \omega), \quad (55)$$

it becomes evident that Eqs. (54) and (55) can be recast as a joint Hermitian eigenvalue problem

$$\mathbf{B}(\vec{k})\mathbf{X}(\vec{k}) = \mathbf{X}(\vec{k})\mathbf{E}(\vec{k}), \quad \mathbf{X}^\dagger(\vec{k})\mathbf{X}(\vec{k}) = 1, \quad (56)$$

$$\mathbf{B}(\vec{k}) = \begin{pmatrix} \bar{F}(\vec{k}) + \bar{\boldsymbol{\Sigma}}^\infty(\vec{k}) & \bar{\mathbf{U}}^{+\dagger}(\vec{k}) & \bar{\mathbf{U}}^{-\dagger}(\vec{k}) \\ \bar{\mathbf{U}}^+(\vec{k}) & \bar{\mathbf{K}}^+(\vec{k}) + \bar{\mathbf{C}}^+(\vec{k}) & \mathbf{0} \\ \bar{\mathbf{U}}^-(\vec{k}) & \mathbf{0} & \bar{\mathbf{K}}^-(\vec{k}) + \bar{\mathbf{C}}^-(\vec{k}) \end{pmatrix}.$$

The new matrix $\mathbf{B}(\vec{k})$ is called the *band structure matrix*. It has to be diagonalized for several \vec{k} points yielding eigenvalues $e_n(\vec{k})=(\mathbf{E}(\vec{k}))_{nn}$ and eigenvectors $\vec{X}_n(\vec{k})=(\vec{x}_G(\vec{k}, e_n(\vec{k}))^\dagger, \bar{x}^+(\vec{k}, e_n(\vec{k}))^\dagger, \bar{x}^-(\vec{k}, e_n(\vec{k}))^\dagger)^\dagger$. Formula (56) is similar to the result for molecules.⁵⁵ One can envisage that the diagonalization of the subblocks $\bar{\mathbf{K}}^\pm(\vec{k})+\bar{\mathbf{C}}^\pm(\vec{k})$ in $\mathbf{B}(\vec{k})$ is

carried out first by solving Eq. (19); afterwards, the full eigenvalue problem (56) is treated with all subblocks modified accordingly.^{55,84} Therefore, via Eq. (15), infinitely many proper self-energy diagrams are summed before the result is put in the Dyson equation (9) to sum all improper self-energy diagrams that derive from those contained in the ADC form.

The spectral representation of the one-particle Green's function (6) reads, in terms of the eigenpairs of the band structure matrix (56),

$$G_{pq}(\vec{k}, \omega) = [\omega 1 - \mathbf{B}(\vec{k})]_{pq}^{-1} = \sum_n \frac{\bar{x}_p^{(n)}(\vec{k})\bar{x}_q^{(n)*}(\vec{k})}{\omega - e_n(\vec{k})}, \quad (57)$$

where $\bar{x}_p^{(n)}(\vec{k})=(\mathbf{X}(\vec{k}))_{pn}$ denotes the transition amplitude of the n th state. It is given by either the $x_p^{(n)}(\vec{k})$ or the $y_p^{(n)}(\vec{k})$ in Eq. (7) whether it belongs to an $N-1$ or an $N+1$ particle state.

In some cases, the external Wannier orbitals of the dynamic self-energy are restricted to a single cell of the crystal—i.e., $\bar{\mathbf{M}}(\vec{k}, \omega) \approx \mathbf{M}(\vec{R}=\vec{0}, \omega)$, the so-called one-lattice-site approximation for the dynamic self-energy. Note, however, that the $2p1h$ and $2h1p$ configurations in neighboring unit cells are not entirely excluded. The \vec{k} dependence, in this approximation, is solely due to the one-particle matrix $\bar{F}(\vec{k})+\bar{\boldsymbol{\Sigma}}^\infty(\vec{k})$. The static self-energy can also be evaluated in one-lattice-site approximation. Then the \vec{k} dependence is exclusively due to $\bar{F}(\vec{k})$ and this approximation to the CO-ADC equations becomes similar to the dynamical mean-field theory.²⁶

VI. CONFIGURATION SELECTION

All equations derived so far contain certain infinite lattice sums that run over the entire crystal forming the configuration space. To obtain a meaningful approximation of the one-particle Green's function, the convergence of those lattice sums must be granted. Sun and Bartlett⁹⁵ study the convergence properties of the lattice sums in several quantum chemical correlation methods for ground states and excited states of crystals, based on the Møller-Plesset partition of the Hamiltonian (2). Following the reasoning of Ref. 95, the lattice sums in CO-ADC in crystal momentum representation converge. Moreover, the equations in local representation also converge as they evolve from the former by means of an inverse Wannier transformation (21b).

Although the convergence of lattice sums is granted principally, we have to devise an algorithm for their proper truncation;⁴ i.e., a dynamical building of the configuration space is required which means to meet a chosen accuracy in the lattice sums for a given crystal. The appropriate truncation of lattice sums is an essential ingredient of all *ab initio* methods for crystals and corresponds to a configuration selection procedure which ensures that the configuration space is sufficiently large for the desired accuracy of the band structure but still sufficiently small to be tractable on present-day computers. In molecular physics, configuration selection has been introduced in the context of the configuration interaction method⁹⁶ which suffers from an exponentially grow-

ing configuration space with respect to the number of atoms in molecules. The techniques discussed in Ref. 96 are not applicable here, as they are designed with the configuration interaction method in mind, but there are analogs for crystals which are similar in spirit.

The incremental scheme for ground states of crystals^{4,6,41,97–101} is based on Wannier orbitals. The total configuration space of a crystal is partitioned into certain subsets which are used in a subsequent calculation of the correlation energy to yield the so-called energy increments. Frequently, explicit manual configuration selection is applied. This allows the partition of the configuration space to be chosen following chemical intuition. Yet the situation is much more cumbersome for band structures because the number of distinct excited states grows with the number of correlated electrons—i.e., the number of Bloch orbitals and Wannier orbitals which are considered in the sums in Eqs. (17) and (29), respectively. In the local Hamiltonian approach, the number of states to be calculated is restricted to a fixed number which is treated in an incremental way.^{32–34,36,40} Albrecht *et al.*^{37,39} ensure the convergence of an incremental series for the self-energy for $\omega=0$, a criterion which is independent of the number of states actually described.

We devise here a configuration selection procedure that is perfectly adapted to the structure of the CO-ADC scheme. For the equations in terms of Bloch orbitals (34) and (17), \vec{k} points are chosen harnessing Born–von Kármán boundary conditions which lead to a net of equidistant \vec{k} points.^{1,3} In this case, configuration selection means choosing a sufficiently dense net in conjunction with a cutoff criterion which is similar to the one for CO-ADC in terms of Wannier orbitals (41) and (29) discussed in the next paragraph. Yet, beforehand, one should interpret the impact of the number of \vec{k} points used for Brillouin zone integration. Using a given net of N_0 \vec{k} points to carry out a Wannier transformation (21a), CO-ADC in terms of Bloch orbitals can be immediately represented and analyzed in terms of the supercell form (25). However, one should emphasize that the redundancies of this representation—which is utilized here for interpretation only—are not present in the Bloch orbital formulation of CO-ADC. The supercell form affords a tight-binding interpretation: within the supercell, the number of distinct neighbors to the origin cell is restricted by the volume of the supercell. Distinct interaction terms among the cells—i.e., the Fock matrix and two-electron integrals—are thus also restricted and the number of \vec{k} points employed can thus be understood to imply the number of nearest-neighbor cells treated in the interaction terms. These arguments generalize the tight-binding arguments given, e.g., in Ref. 80, in conjunction with a single Brillouin zone integration of a crystal-momentum-dependent function to the multidimensional case.

Configuration selection in crystal momentum representation is not intuitive and does not allow a fine-grained selection of configurations within unit cells and between an origin cell and its neighbor cells. For crystals with large unit cells this is a significant restriction. To obtain a suitable cutoff criterion for CO-ADC in terms of Wannier orbitals (41) and (29), we evaluate the second-order diagram of the retarded

dynamic self-energy^{41,50,55} and examine the summand therein:

$$\frac{V_{0\vec{q}\vec{g}_1\kappa[\vec{g}_2\alpha\vec{g}_3\beta]}^* V_{R\sigma\vec{g}_1\kappa[\vec{g}_2\alpha\vec{g}_3\beta]}}{\omega - \varepsilon_{\vec{g}_2\alpha} - \varepsilon_{\vec{g}_3\beta} + \varepsilon_{\vec{g}_1\kappa}} n_{\vec{g}_1\kappa} \bar{n}_{\vec{g}_2\alpha} \bar{n}_{\vec{g}_3\beta}. \quad (58)$$

The most delocalized occupied orbitals are the valence orbitals. Therefore, the occupied valence orbitals couple to the most important $2p1h$ configurations. Hence, ω can be assumed to be of the order of the band gap. The denominator in Eq. (58) is regarded to be constant to a reasonable degree. It is thus considered as being part of the cutoff threshold.

Therefore, if $V_{0\vec{q}\vec{g}_1\kappa[\vec{g}_2\alpha\vec{g}_3\beta]}^* V_{R\sigma\vec{g}_1\kappa[\vec{g}_2\alpha\vec{g}_3\beta]}$ is above a certain cutoff threshold for some combination of $\vec{0}\vec{q}$ and $\vec{R}\sigma$, we include the corresponding $2p1h$ test configuration $(\vec{g}_1\kappa, \vec{g}_2\alpha, \vec{g}_3\beta)$ in the configuration space. If the product is small for all external Wannier orbitals of the self-energy, $(\vec{g}_1\kappa, \vec{g}_2\alpha, \vec{g}_3\beta)$ is neglected completely by setting all two-electron integrals containing this configuration exactly to zero. By this, only a finite range of the residual Coulomb interaction, which is not treated in Hartree-Fock approximation, is explored. The same arguments hold for the selection of $2h1p$ configurations for the evaluation of the advanced dynamic self-energy, if Eq. (58) is adapted in the same way as Eq. (32) is adapted to \bar{U}^- , \bar{K}^- , and \bar{C}^- .

Convergence of the configuration space—i.e., the number of unit cells contributing configurations to be considered in the cutoff criterion (58)—is expected to be sufficiently quick. Van der Waals dispersion interactions which are present both in the ground state of the N particle system and the states of the $(N\pm 1)$ -particle system are nearly equal and thus almost cancel in band structure calculations. However, the effect of the extra Coulomb charge that arises in $(N\pm 1)$ -particle states in contrast to the N -particle ground state is long range. The potential of an extra point charge falls off like $V(r) = \pm 1/(\varepsilon r)$, where ε is the dielectric constant of the solid. This causes an overall polarization of the crystal which can be accounted for by adjusting the chemical potential μ^\pm of the added or removed electron accordingly by using a continuum approximation.^{4,32,33,36} This procedure is not specific to the CO-ADC theory advocated here to treat the short-range interactions, but is required generally.

Having introduced a convenient method to truncate the configuration space for CO-ADC, we have to elucidate the physical impact of configuration selection on band structures. To this end, we consider the fully translational symmetry adapted form (29). The modified coupling amplitudes (29b) in the band structure matrix (56) of a crystal carry two independent crystal lattice vectors \vec{g}'_1 and \vec{g}'_2 . If \vec{g}'_1 and \vec{g}'_2 are sufficiently far away from the origin cell, all two-electron matrix elements (32a) which contribute to the modified coupling amplitude $\bar{U}_{\sigma;\vec{g}'_1\vec{g}'_2\kappa'\alpha'\beta'}^+(\vec{k})$ fall for all σ below the configuration selection threshold and are therefore zero. Because the modified interaction matrices (32c) vanish in the CO-ADC(2,2) approximation and Eq. (29c) thus denotes a diagonal matrix, the eigenvalue associated with the configuration $(\vec{g}'_1\vec{g}'_2\kappa'\alpha'\beta')$ is simply given by the diagonal element

$(\vec{K}^\pm(\vec{k}))_{\vec{g}'_1\vec{g}'_2\kappa'\alpha'\beta';\vec{g}'_1\vec{g}'_2\kappa'\alpha'\beta'}$, with an eigenvector being unity on position $\vec{g}'_1\vec{g}'_2\kappa'\alpha'\beta'$ and zero elsewhere. Consequently, such an eigenstate of $\mathbf{B}(\vec{k})$ is removed by deleting the column and the row $\vec{g}'_1\vec{g}'_2\kappa'\alpha'\beta'$ in $\mathbf{B}(\vec{k})$ because the transition amplitude (7) vanishes and thus it does not contribute to the spectral representation of the one-particle Green's function (57).

A further consequence of configuration selection involves the lattice summations over \vec{R} in Eqs. (29b) and (29c). In the first place, we consider a crystal with a macroscopic lattice constant which consists of N_0 unit cells. As a result, only Fock and two-electron matrix elements that involve Wannier orbitals from the origin cell are selected. Therefore, in Eqs. (29b) and (29c), the lattice sums run over only the single term for $\vec{R}=\vec{0}$ with $\vec{g}_1=\vec{g}_2=\vec{0}$ and the resulting band structure matrix (56) is consequently independent of \vec{k} . As the Brillouin zone contains N_0 crystal momenta, we obtain a N_0 -fold degenerate spectrum similarly to simple tight-binding models.¹ In typical crystals, interactions with neighboring unit cells are important. Yet a sufficiently large supercell which consist of n_0 unit cells can be chosen such that interactions between supercells are negligible leading to a N_0/n_0 -fold degenerate spectrum. In other words, a cutoff threshold, to be used for the selection of Fock matrix elements and $2p1h$ and $2h1p$ configurations, implies a definition of degeneracy of the physical states in our model of the crystal.

In order to selectively diagonalize the band structure matrix, one uses an iterative eigenvalue solver—e.g., a block-Lanczos algorithm^{84,94,102,103}—that is capable of exploiting the sparsity of $\mathbf{B}(\vec{k})$. The most expensive step of the block-Lanczos algorithm is a matrix times vector product¹¹⁷ between $\mathbf{B}(\vec{k})$ and Lanczos vectors which determines the overall performance of the eigenvalue solver.^{84,94,103,104} To investigate the scaling of a selective computation of eigenpairs, we consider a supercell consisting of two unit cells of an original lattice. Let us assume a crystal with a macroscopic lattice constant to investigate the asymptotic scaling behavior of the problem. Then, the configuration selection method of the previous paragraphs selects only configurations local to the individual unit cells. Hence, the resulting configuration space scales linearly with the system size—i.e., the number of atoms per unit cell. This is a necessary condition for the selective diagonalization of the band structure matrix (56) to scale linearly as well. The total Fock matrix of the supercell also is block diagonal. Similarly, the modified coupling amplitudes (29b) only contain two nonzero blocks which describe the coupling of $2p1h$ and $2h1p$ configurations to the Fock matrix of each of the two constituting unit cells of the supercell such that the total band structure matrix decomposes into two subproblems that can be solved independently. A single matrix times vector product for the supercell requires twice as many floating point operations than are needed for a matrix times vector product for one of the two unit cells in the supercell. Hence, the computation of matrix times vector products scales linearly with the system size.¹¹⁸ Yet doubling the system size also usually means that we are interested in twice as many excited states. Hence, the

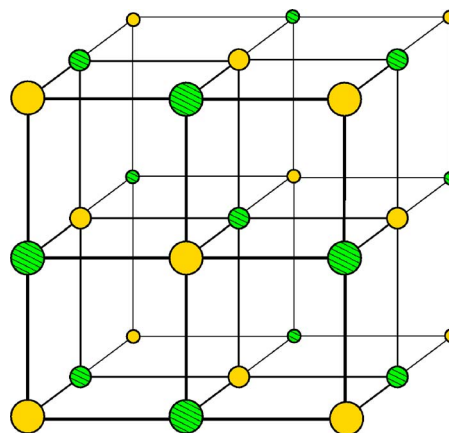


FIG. 1. (Color online) Structure of a LiF crystal. The lithium and fluorine atoms are represented by solid yellow and hatched green spheres, respectively.

overall effort to determine all excited states of a crystal in a given energy range scales quadratically. It is a *quadratically* scaling problem, where linear scaling can only be achieved by an *a priori* restriction to a few excited states of the system.

For typical crystals, the Fock matrix of a supercell is not block diagonal which implies another doubling of the number of floating point operations upon doubling the system size. Yet this factor cancels as the number of \vec{k} points needed for a given accuracy of the integration over the Brillouin zone of the supercell is halved because the volume of its Brillouin zone is half the volume of the Brillouin zone which corresponds to the original crystal lattice.¹

VII. LITHIUM FLUORIDE CRYSTAL

Lithium fluoride crystallizes in a face-centered-cubic (fcc) rocksalt structure described by the space group $Fm\bar{3}m$ as shown in Fig. 1. The crystal lattice has a two-atomic basis Li(0,0,0) and F(1/2, 1/2, 1/2), given in units of the lattice constant¹¹⁹ $a=3.990$ Å. To investigate a LiF crystal, we have chosen the simplest possible *ab initio* description. The main purpose here is to demonstrate the feasibility of the CO-ADC formulas for a three-dimensional crystalline solid. Thus, only a minimal Gaussian STO-6G basis set^{105,106} is used which describes the lithium atom by a $(12s)/[2s]$ contraction and the fluorine atom by $(12s\ 6p)/[2s\ 1p]$. Each shell of the STO-6G basis set is constructed by fitting six Gaussian functions to each occupied orbital of the isolated atoms.¹⁰⁵ The $2s$ shell of a lithium atom is rather diffuse due to the single outer valence electron. As the lithium atoms are ionized in LiF crystals, we remove the two most diffuse Gaussian functions in the Li $2s$ contraction because they do not reflect the physical situation of a compact Li⁺ ion, and arrive at a $(10s)/[2s]$ contraction scheme.

The Hartree-Fock equations are solved self-consistently by means of the WANNIER program^{42,43} which directly yields Wannier orbitals. A finite cluster of unit cells is utilized as support for the Wannier orbitals of the origin cell which, in

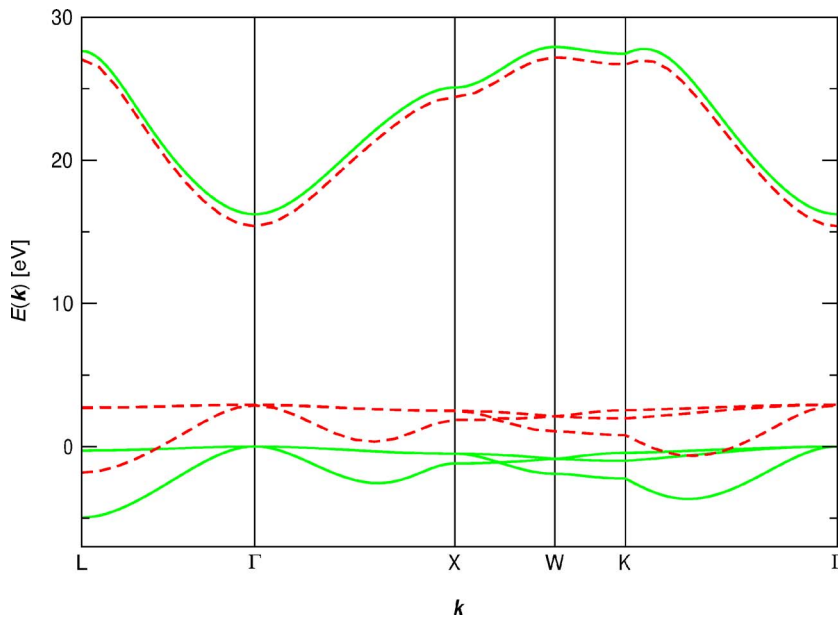


FIG. 2. (Color online) Band structure of a LiF crystal. Hartree-Fock bands are given by solid green lines. The dashed red lines depict the CO-ADC(2,2) quasiparticle bands which are determined by accounting for $2p1h$ and $2h1p$ configurations involving Wannier orbitals in the origin cell and the nearest- and next-nearest-neighbor cells.

our case, consist of up to third-nearest-neighbor cells (43 unit cells altogether). As the program determines only occupied Wannier orbitals, crystal projected atomic orbitals^{41,107,120} (crystal PAOs) have been devised on the basis of the projected atomic orbitals introduced by Saebø and Pulay^{108,109} and also used by Hampel and Werner.¹¹⁰ The resulting virtual functions are subsequently Löwdin orthonormalized.^{10,11,77,78} For the CO-ADC(2,2) method (29), (32), and (56), the Fock matrix and the two-electron integrals in Wannier representation, entering the Hamiltonian (31), need to be obtained by a transformation of the corresponding quantities in terms of Gaussian basis functions. This transformation is presently the bottleneck in practical computations since the WANNIER program^{42,43} carries it out for clusters only and neither uses translational nor point group symmetry. At present, this permits only the use of a minimal basis set for a three-dimensional LiF crystal. The

subsequent correlation calculations with the CO-ADC program^{41,111} are very efficient and as rapid as typical molecular ADC calculations.

The Hartree-Fock band structure that results from this minimal basis is shown in Fig. 2. All band energies are given with respect to the top of the valence bands which is located at the Γ point and is set to zero. Below zero there is a complex of three F $2p$ valence bands shown as a closeup in Fig. 3. They originate from the three F $2p$ valence energy levels of the LiF molecule around 12 eV where the lowest ionization potential of the molecule is doubly degenerate.⁴¹ Upon crystallization, this degeneracy is lifted due to interactions with neighboring atoms and, except for the high-symmetry lines Γ -L and Γ -X, one observes three distinct F $2p$ valence bands. As a minimal basis set is utilized, there is only a single conduction band of mainly Li $2s$ character. A slight admixture of F $2p$ character to this band is observed in the

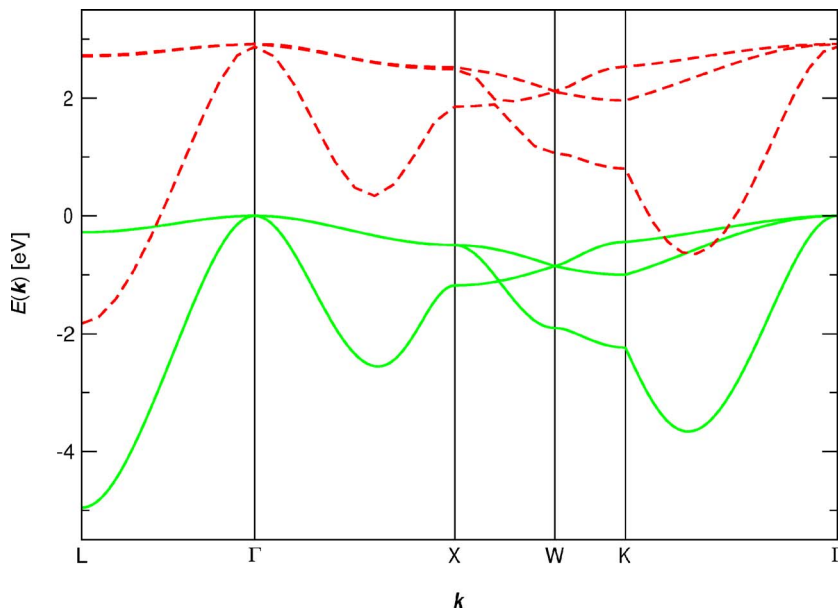


FIG. 3. (Color online) Valence-band structure of a LiF crystal. Zoom into Fig. 2.

TABLE I. Convergence of the top of the valence bands $E_{\text{top},v}$, the bottom of the conduction band $E_{\text{bottom},c}$, the fundamental band gap E_{gap} , and the bandwidth of the F $2p$ valence band complex ΔE_{F2p} of a LiF crystal. "Cells" designates the number of unit cells taken into account in CO-ADC(2,2) calculations of the quasiparticle band structure where zero refers to the Hartree-Fock result. Unity denotes the inclusion of the $2p1h$ and $2h1p$ configurations from the origin cell only in correlation calculations. "13" and "19" indicate the additional inclusion of configurations from nearest- and next-nearest-neighbor cells, respectively. For a LiF crystal, $E_{\text{top},v}$ and $E_{\text{bottom},c}$ are both situated at the Γ point. All data are given in electronvolts.

Cells	$E_{\text{top},v}$	$E_{\text{bottom},c}$	E_{gap}	ΔE_{F2p}
0	0	16.24	16.24	4.95
1	0.41	16.16	15.74	4.80
13	2.43	15.69	13.26	4.78
19	2.89	15.36	12.47	4.75

W - K panel by comparing with the band structure resulting from a larger basis set—e.g., the one of Ref. 38, where a conduction band of F $2p$ character mixes with the Li $2s$ band. Nevertheless, the single conduction band represents the energetically lower edge of the conduction-band complex well. LiF has a direct band gap; i.e., the maximum of the F $2p$ valence bands and the minimum of the Li $2s$ conduction band are located at the same crystal momentum, the Γ point, here.

In order to investigate electron correlations, we start from a single unit cell, to form the $2p1h$ and $2h1p$ configurations entering Eq. (29) for $M^\pm(\vec{k}, \omega)$, respectively. Successively, configurations which contain Wannier orbitals in nearest- and next-nearest-neighbor cells are considered. This leads to three distinct quasiparticle band structures whose convergence with respect to the number of unit cells where electron correlations are regarded explicitly is monitored for the following key quantities: the top of the valence bands, the bottom of the conduction band, and the band gap and width of the F $2p$ valence-band complex (Table I). The results are compared with the plain Hartree-Fock data (with configurations out of "0" unit cells). Taking into account electron correlations of a single unit cell causes a slight upwards shift of the valence bands by 0.41 eV while the conduction band essentially remains unchanged. Upon inclusion of configurations in the nearest-neighbor cells, the band structure changes drastically, leading to a significant reduction of the band gap by 2.48 eV. Accounting for configurations which extend to next-nearest-neighbor cells has three times less impact on the band gap. Therewith, it can clearly be seen that the major contributions of electron correlations have been covered and that the effect of configurations which extend to Wannier orbitals beyond next-nearest-neighbor cells will yield much less significant changes of the quantities than those discernible in Table I. As pointed out in Sec. VI, the effect of the more distant unit cells can be determined using a continuum approximation.^{4,32,33,36} The observed correlation corrections in Table I with a growing number of neighboring unit cells result primarily from the formation of a quasipar-

ticle and the polarization of the surrounding by the Coulomb charge of the added particle or hole.⁴ Note that, additionally, the beneficial basis set extension^{2,5,112} (BSE) effect is noticeable in solids which leads to an improved description of electron correlations with an increasing number of unit cells taken into account.

The quasiparticle band structure of LiF is displayed in Fig. 2 for the F $2p$ valence bands and the Li $2s$ conduction band. The former bands are additionally displayed on an enlarged scale in Fig. 3. The data are taken from the computation with configurations from altogether 19 unit cells. Valence and conduction bands do not shift by the same amount, upwards and downwards, respectively. Instead, the former bands are much more strongly influenced by electron correlations than the latter bands. This is due to the fact that the occupied Wannier orbitals are spatially less extended than the virtual Wannier orbitals. For electrons in compact orbitals, the Hartree-Fock approximation becomes progressively worse due to an insufficient description of the Coulomb hole.⁴ Although the quasiparticle bands are considerably shifted with respect to the corresponding Hartree-Fock bands, they essentially keep their width. We also observe this effect for $(\text{HF})_\infty$ chains.⁴¹ This is in contrast to the significant reduction of bandwidths observed for quasiparticle band structures of covalently bonded polymers like *trans*-polyacetylene⁴⁰ and covalently bonded crystals like diamond,^{32,33,36} silicon,^{33,36} and germanium.³³

The *ab initio* description of a LiF crystal using a minimal basis set provides valuable insights. However, we cannot expect full quantitative agreement neither at the Hartree-Fock nor at the correlation level. The accuracy of our approach can be determined by comparing with experimental and theoretical data from related studies. The fundamental band gap is accessible by photoelectron spectroscopy and has been measured to be 14.1 eV. Another experimentally accessible quantity, the width of the F $2p$ valence-band complex, was determined to lie in the range⁷⁰ of 3.5–6 eV and thus is inconclusive, unfortunately. With our STO-6G-like basis set, we find a Hartree-Fock band gap of 16.24 eV (Table I) which deviates considerably from the value of 22.7 eV communicated by Kunz⁷⁰ or the value of 22.4 eV reported by Albrecht³⁸ who both use larger basis sets. For the width of the F $2p$ valence-band complex, we find 4.95 eV (Table I) in the Hartree-Fock approximation which is appreciably larger than the value of 3 eV from Kunz⁷⁰ and the value of 3.37 eV from Albrecht.³⁸

Including electron correlations, the quasiparticle band gap reduces to 12.47 eV (Table I) and thus falls short by 1.5 eV compared to the experimental value. Albrecht³⁸ finds 13.5 eV, and calculations of Kunz⁷⁰ yield a theoretical band gap of 14.0 eV, in good agreement with the recent measurements of 14.1 eV. For the F $2p$ valence-band complex, we obtain a width of 4.75 eV (Table I) which is nearly unchanged compared to the Hartree-Fock value, a fact that has also been found in previous studies of bulk LiF.^{38,70} Consequently, our value of the width remains much higher than the value of 3.1 eV from Kunz⁷⁰ or the value of 3.40 eV from Albrecht.³⁸

The above results show that the CO-ADC theory can be applied without problems to compute the energy bands of three-dimensional crystalline solids. What remains to be im-

proved considerably is the transformation of the Fock matrix and the two-electron integrals from the Gaussian basis set representation to a representation in terms of Wannier orbitals.

VIII. CONCLUSION

In this article, a general local orbital *ab initio* Green's function method is devised for band structures. The band structure is given by the pole positions of the one-particle Green's function in terms of Bloch orbitals which in turn is evaluated efficiently utilizing Dyson's equation. To approximate the self-energy up to n th order, we devise a crystal orbital formulation of the well-established algebraic diagrammatic construction (ADC) (Refs. 54–56) which is termed crystal orbital ADC (CO-ADC).⁸⁹ The pole search of the one-particle Green's function is recast into a Hermitian eigenvalue problem which is a numerically stable and efficient formulation, permitting us to explore strong correlations that occur for the energetically lower-lying bands of crystals.^{1,10–14} Wannier orbitals are used in internal summations in the self-energy and allow us to exploit the fact that electron correlations are predominantly local.

The lattice summations in the CO-ADC equations must be truncated to render the problem tractable. To this end, we devise a configuration selection procedure which can equally well be used in conjunction with the calculation of ionization potentials and electron affinities of large molecules to speed up computations. Configuration selection is shown to lead to a definition of degeneracy among the states of a crystal.

The derivation of the local orbital CO-ADC theory sets out from the equations in terms of Bloch orbitals. Afterwards internal indices are transformed to a Wannier representation. We consider this line of argument to be compelling due to the close analogy of the equations in crystal momentum representation to the equations of molecular physics. Alternatively, the derivation can be conducted by starting from CO-ADC in terms of Wannier orbitals. A transformation of the

equations to crystal momentum representation is then carried out by utilizing the Wannier transformation (21a).

The CO-ADC computer program^{41,111} has been developed for computations based on the CO-ADC(2,2) approximation. It requires the Fock matrix and the two-electron integrals in local representation which are obtained by an integral transformation using the Wannier orbitals from a Hartree-Fock calculation with the *ab initio* program WANNIER.^{42,43} At present, this transformation poses a bottleneck because the current implementation has been designed for molecular clusters and does not exploit any symmetries. Therefore, only a minimal basis set is used to study a lithium fluoride crystal in order to demonstrate that the method is working. A fundamental band gap of 12.47 eV and a bandwidth of the F $2p$ valence-band complex of 4.75 eV is obtained. These values are to compare with the experimental data of 14.1 eV, and 3.5–6 eV and the theoretical results of 13.5, 14.0 eV and 3.1, 3.4 eV for the band gap and the bandwidth, respectively. Increasing the size of the basis set will improve the CO-ADC(2,2) results. Yet it is demonstrated that the CO-ADC theory is well suited for tackling the problem of calculating energy bands of solids with controlled approximations.

We would like to point out that the block of $2p1h$ configurations in the band structure matrix (56) is much larger than the block of $2h1p$ configurations. In order to reduce the computational effort, the advanced part and the retarded part of the one-particle Green's function can be independently evaluated diagrammatically. This leads to a different, so-called non-Dyson CO-ADC scheme, which decouples the computation of occupied and virtual bands completely^{93,113} and results in two independent Hermitian matrix eigenvalue problems to be solved.

ACKNOWLEDGMENTS

We would like to thank Jochen Schirmer for fruitful discussions and critically reading the manuscript. C.B. is indebted to Thomas Sommerfeld for providing his complex-symmetric block-Lanczos algorithm and helpful advice.

*Corresponding author. Electronic address: Christian.Buth@web.de

†Present address: Theoretische Chemie, Universität Siegen, 57068 Siegen, Germany.

¹N. W. Ashcroft and N. D. Mermin, *Solid State Physics* (Cole, London, 1976).

²C. Pisani, R. Dosevi, and C. Roetti, *Hartree-Fock ab initio Treatment of Crystalline Systems*, Vol. 48 of Lecture Notes in Chemistry (Springer, Berlin, 1988).

³J. Callaway, *Quantum Theory of the Solid State*, 2nd ed. (Academic Press, Boston, 1991).

⁴P. Fulde, *Electron Correlations in Molecules and Solids*, 3rd ed., Vol. 100 of *Springer Series in Solid-State Sciences* (Springer, Berlin, 1995).

⁵Quantum-Mechanical *ab initio* Calculation of the Properties of Crystalline Materials, edited by C. Pisani, Vol. 67 of *Lecture Notes in Chemistry* (Springer, Berlin, 1996).

⁶P. Fulde, *Adv. Phys.* **51**, 909 (2002).

⁷P. Hohenberg and W. Kohn, *Phys. Rev.* **136**, B864 (1964).

⁸W. Kohn and L. J. Sham, *Phys. Rev.* **140**, A1133 (1965).

⁹W. Y. Ching, F. Gan, and M.-Z. Huang, *Phys. Rev. B* **52**, 1596 (1995).

¹⁰P.-O. Löwdin, *Adv. Phys.* **5**, 1 (1956).

¹¹P.-O. Löwdin, *J. Appl. Phys.* **33**, 251 (1962).

¹²L. S. Cederbaum, W. Domcke, J. Schirmer, and W. von Niessen, in *Advances in Chemical Physics*, edited by I. Prigogine and S. A. Rice (John Wiley & Sons, New York, 1986), Vol. 65, pp. 115–159.

¹³C. Buth, R. Santra, and L. S. Cederbaum, *J. Chem. Phys.* **119**, 7763 (2003).

¹⁴C. Buth, R. Santra, and L. S. Cederbaum, *J. Chem. Phys.* **119**, 10575 (2003).

¹⁵L. Hedin, *Phys. Rev.* **139**, A796 (1965).

- ¹⁶R. Hott, Phys. Rev. B **44**, 1057 (1991).
- ¹⁷V. I. Anisimov, F. Aryasetiawan, and A. I. Lichtenstein, J. Phys.: Condens. Matter **9**, 767 (1997).
- ¹⁸T. Grabo, T. Kreibich, S. Kurth, and E. K. U. Gross, in *Strong Coulomb Correlations in Electronic Structure Calculations*, edited by V. I. Anisimov (Taylor & Francis, London, 2000), pp. 203–311.
- ¹⁹M. Städele, M. Moukara, J. A. Majewski, P. Vogl, and A. Görling, Phys. Rev. B **59**, 10031 (1999).
- ²⁰Y. Kakehashi, Phys. Rev. B **45**, 7196 (1992).
- ²¹Y. Kakehashi, Phys. Rev. B **65**, 184420 (2002).
- ²²W. Metzner and D. Vollhardt, Phys. Rev. Lett. **62**, 324 (1989).
- ²³W. Metzner and D. Vollhardt, Phys. Rev. Lett. **62**, 1066 (1989).
- ²⁴E. Müller-Hartmann, Z. Phys. B: Condens. Matter **74**, 507 (1989).
- ²⁵T. Pruschke, M. Jarrell, and J. K. Freericks, Adv. Phys. **44**, 187 (1995).
- ²⁶A. Georges, G. Kotliar, W. Krauth, and M. J. Rozenberg, Rev. Mod. Phys. **68**, 13 (1996).
- ²⁷M. Jarrell and H. R. Krishnamurthy, Phys. Rev. B **63**, 125102 (2001).
- ²⁸L. D. Faddeev, Sov. Phys. JETP **12**, 1014 (1961).
- ²⁹P. Unger, J. Igarashi, and P. Fulde, Phys. Rev. B **50**, 10485 (1994).
- ³⁰W. M. C. Foulkes, L. Mitas, R. J. Needs, and G. Rajagopal, Rev. Mod. Phys. **73**, 33 (2001).
- ³¹J. J. Ladik, *Quantum Theory of Polymers as Solids* (Plenum Press, New York, 1988).
- ³²J. Gräfenstein, H. Stoll, and P. Fulde, Chem. Phys. Lett. **215**, 611 (1993).
- ³³J. Gräfenstein, H. Stoll, and P. Fulde, Phys. Rev. B **55**, 13588 (1997).
- ³⁴M. Albrecht, P. Reinhardt, and J.-P. Malrieu, Theor. Chem. Acc. **100**, 241 (1998).
- ³⁵J. J. Ladik, Phys. Rep. **313**, 171 (1999).
- ³⁶M. Albrecht, P. Fulde, and H. Stoll, Chem. Phys. Lett. **319**, 355 (2000).
- ³⁷M. Albrecht and J. Igarashi, J. Phys. Soc. Jpn. **70**, 1035 (2001).
- ³⁸M. Albrecht, Theor. Chem. Acc. **107**, 71 (2002).
- ³⁹M. Albrecht and P. Fulde, Phys. Status Solidi B **234**, 313 (2002).
- ⁴⁰V. Bezugly and U. Birkenheuer, Chem. Phys. Lett. **399**, 57 (2004).
- ⁴¹C. Buth, Dissertation, Technische Universität Dresden, Germany, 2005.
- ⁴²A. Shukla, M. Dolg, H. Stoll, and P. Fulde, Chem. Phys. Lett. **262**, 213 (1996).
- ⁴³A. Shukla, M. Dolg, P. Fulde, and H. Stoll, Phys. Rev. B **57**, 1471 (1998).
- ⁴⁴Y. Toyozawa, Prog. Theor. Phys. **12**, 422 (1954).
- ⁴⁵S. Suhai, Phys. Rev. B **27**, 3506 (1983).
- ⁴⁶J.-Q. Sun and R. J. Bartlett, J. Chem. Phys. **104**, 8553 (1996).
- ⁴⁷S. Hirata and R. J. Bartlett, J. Chem. Phys. **112**, 7339 (2000).
- ⁴⁸R. Pino and G. E. Scuseria, J. Chem. Phys. **121**, 2553 (2004).
- ⁴⁹L. S. Cederbaum, J. Phys. B **8**, 290 (1975).
- ⁵⁰L. S. Cederbaum and W. Domcke, in *Advances in Chemical Physics*, edited by I. Prigogine and S. A. Rice (John Wiley & Sons, New York, 1977), Vol. 36, pp. 205–344.
- ⁵¹W. von Niessen, J. Schirmer, and L. S. Cederbaum, Comput. Phys. Rep. **1**, 57 (1984).
- ⁵²C.-M. Liegener, J. Phys. C **18**, 6011 (1985).
- ⁵³J. I. Igarashi, P. Unger, K. Hirai, and P. Fulde, Phys. Rev. B **49**, 16181 (1994).
- ⁵⁴J. Schirmer, Phys. Rev. A **26**, 2395 (1982).
- ⁵⁵J. Schirmer, L. S. Cederbaum, and O. Walter, Phys. Rev. A **28**, 1237 (1983).
- ⁵⁶L. S. Cederbaum, in *Encyclopedia of Computational Chemistry*, edited by P. v. R. Schleyer (John Wiley & Sons, Chichester, 1998), Vol. 2, pp. 1202–1211.
- ⁵⁷M. S. Deleuze and L. S. Cederbaum, Phys. Rev. B **53**, 13326 (1996).
- ⁵⁸A. Golod, M. S. Deleuze, and L. S. Cederbaum, J. Chem. Phys. **110**, 6014 (1999).
- ⁵⁹R. Santra, J. Zobeley, and L. S. Cederbaum, Phys. Rev. B **64**, 245104 (2001).
- ⁶⁰J. Schirmer and G. Angonoa, J. Chem. Phys. **91**, 1754 (1989).
- ⁶¹R. Santra and L. S. Cederbaum, J. Chem. Phys. **117**, 5511 (2002).
- ⁶²J. Schirmer, Phys. Rev. A **43**, 4647 (1991).
- ⁶³J. Schirmer and F. Mertins, Int. J. Quantum Chem. **58**, 329 (1996).
- ⁶⁴F. Mertins and J. Schirmer, Phys. Rev. A **53**, 2140 (1996).
- ⁶⁵E. L. Shirley, L. J. Terminello, J. E. Klepeis, and F. J. Himpsel, Phys. Rev. B **53**, 10296 (1996).
- ⁶⁶M. Piacentini, D. W. Lynch, and C. G. Olson, Phys. Rev. B **13**, 5530 (1976).
- ⁶⁷R. W. G. Wyckoff, *Crystal Structures*, 2nd ed. (Wiley, New York, 1968), Vol. I.
- ⁶⁸R. T. Poole, J. G. Jenkin, J. Liesegang, and R. C. G. Leckey, Phys. Rev. B **11**, 5179 (1975).
- ⁶⁹R. T. Poole, J. Liesegang, R. C. G. Leckey, and J. G. Jenkin, Phys. Rev. B **11**, 5190 (1975).
- ⁷⁰A. B. Kunz, Phys. Rev. B **26**, 2056 (1982).
- ⁷¹M. Prencipe, A. Zupan, R. Dovesi, E. Aprà, and V. R. Saunders, Phys. Rev. B **51**, 3391 (1995).
- ⁷²K. Doll and H. Stoll, Phys. Rev. B **56**, 10121 (1997).
- ⁷³N.-P. Wang, M. Rohlfing, P. Krüger, and J. Pollmann, Phys. Rev. B **67**, 115111 (2003).
- ⁷⁴G. Del Re, J. J. Ladik, and G. Biczó, Phys. Rev. **155**, 997 (1967).
- ⁷⁵J.-M. André, L. Gouverneur, and G. Leroy, Int. J. Quantum Chem. **1**, 427 (1967).
- ⁷⁶J.-M. André, L. Gouverneur, and G. Leroy, Int. J. Quantum Chem. **1**, 451 (1967).
- ⁷⁷A. Szabo and N. S. Ostlund, *Modern Quantum Chemistry: Introduction to advanced electronic structure theory*, 1st ed. (revised) (McGraw-Hill, New York, 1989).
- ⁷⁸R. McWeeny, *Methods of Molecular Quantum Mechanics*, 2nd ed. (Academic Press, London, 1992).
- ⁷⁹T. Helgaker, P. Jørgensen, and J. Olsen, *Molecular Electronic Structure Theory* (John Wiley & Sons, Chichester, 2000).
- ⁸⁰H. J. Monkhorst and J. D. Pack, Phys. Rev. B **13**, 5188 (1976).
- ⁸¹R. D. Mattuck, *A Guide to Feynman Diagrams in the Many-Body Problem*, 2nd ed. (McGraw-Hill, New York, 1976).
- ⁸²A. L. Fetter and J. D. Walecka, *Quantum Theory of Many-Particle Systems*, International Series in Pure and Applied Physics, edited by Leonard I. Schiff (McGraw-Hill, New York, 1971).
- ⁸³E. K. U. Gross, E. Runge, and O. Heinonen, *Many-Particle Theory* (Adam Hilger, Bristol, 1991).
- ⁸⁴H.-G. Weikert, H.-D. Meyer, L. S. Cederbaum, and F. Tarantelli, J. Chem. Phys. **104**, 7122 (1996).
- ⁸⁵C. Pisani and U. Birkenheuer, Comput. Phys. Commun. **96**, 152

- (1996).
- ⁸⁶U. Birkenheuer, F. Corà, C. Pisani, E. Scorzà, and G. Perego, *Surf. Sci.* **373**, 393 (1997).
- ⁸⁷S. Ethofer and P. Schuck, *Z. Phys.* **228**, 264 (1969).
- ⁸⁸J. Winter, *Nucl. Phys. A* **194**, 535 (1972).
- ⁸⁹M. S. Deleuze, *Int. J. Quantum Chem.* **93**, 191 (2003).
- ⁹⁰G. H. Wannier, *Phys. Rev.* **52**, 191 (1937).
- ⁹¹N. Marzari and D. Vanderbilt, *Phys. Rev. B* **56**, 12847 (1997).
- ⁹²C. M. Zicovich-Wilson, R. Dovesi, and V. R. Saunders, *J. Chem. Phys.* **115**, 9708 (2001).
- ⁹³U. Birkenheuer and C. Buth (unpublished).
- ⁹⁴G. H. Golub and C. F. van Loan, *Matrix Computations*, 3rd ed. (Johns Hopkins University Press, Baltimore, 1996).
- ⁹⁵J.-Q. Sun and R. J. Bartlett, *J. Chem. Phys.* **106**, 5554 (1997).
- ⁹⁶R. J. Buenker and S. D. Peyerimhoff, *Theor. Chim. Acta* **35**, 33 (1974).
- ⁹⁷H. Stoll, *Chem. Phys. Lett.* **191**, 548 (1992).
- ⁹⁸H. Stoll, *Phys. Rev. B* **46**, 6700 (1992).
- ⁹⁹H. Stoll, *J. Chem. Phys.* **97**, 8449 (1992).
- ¹⁰⁰C. Willnauer and U. Birkenheuer, *J. Chem. Phys.* **120**, 11910 (2004).
- ¹⁰¹C. Buth and B. Paulus, *Chem. Phys. Lett.* **398**, 44 (2004).
- ¹⁰²C. Lanczos, *J. Res. Natl. Bur. Stand.* **45**, 255 (1950).
- ¹⁰³J. K. Cullum and R. A. Willoughby, *Lanczos Algorithms for Large Symmetric Eigenvalue Computations* (Birkhäuser, Boston, 1985).
- ¹⁰⁴C. Buth, R. Santra, and L. S. Cederbaum, *Phys. Rev. A* **69**, 032505 (2004).
- ¹⁰⁵W. J. Hehre, R. F. Stewart, and J. A. Pople, *J. Chem. Phys.* **51**, 2657 (1969).
- ¹⁰⁶Basis sets were obtained from the Extensible Computational Chemistry Environment Basis Set Database, version 02/25/04, as developed and distributed by the Molecular Science Computing Facility, Environmental and Molecular Sciences Laboratory which is part of the Pacific Northwest Laboratory, P.O. Box 999, Richland, Washington 99352, USA, and funded by the U.S. Department of Energy. The Pacific Northwest Laboratory is a multiprogram laboratory operated by Battelle Memorial Institute for the U.S. Department of Energy under Contract No. DE-AC06-76RLO 1830. Contact David Feller or Karen Schuchardt for further information. <http://www.emsl.pnl.gov/forms/basisform.html>
- ¹⁰⁷A. Shukla, M. Dolg, P. Fulde, and H. Stoll, *Phys. Rev. B* **60**, 5211 (1999).
- ¹⁰⁸P. Pulay, *Chem. Phys. Lett.* **100**, 151 (1983).
- ¹⁰⁹S. Saebø and P. Pulay, *Annu. Rev. Phys. Chem.* **44**, 213 (1993).
- ¹¹⁰C. Hampel and H.-J. Werner, *J. Chem. Phys.* **104**, 6286 (1996).
- ¹¹¹C. Buth, *CO-ADC user's manual*, Max-Planck-Institut für Physik komplexer Systeme, Nöthnitzer Strasse 38, 01187 Dresden, Germany, 2004, with contributions by Martin Albrecht, Hans-Dieter Meyer, Uwe Riss, and Thomas Sommerfeld.
- ¹¹²F. B. van Duijneveldt, J. G. C. M. van Duijneveldt-van de Rijdt, and J. H. van Lenthe, *Chem. Rev. (Washington, D.C.)* **94**, 1873 (1994).
- ¹¹³J. Schirmer, A. B. Trofimov, and G. Stelter, *J. Chem. Phys.* **109**, 4734 (1998).
- ¹¹⁴D. M. Roessler and W. C. Walker, *J. Phys. Chem. Solids* **28**, 1507 (1967).
- ¹¹⁵M. Piacentini, *Solid State Commun.* **17**, 697 (1975).
- ¹¹⁶The experimental band gap of LiF is communicated in the early work of Roessler and Walker to be 13.60 ± 0.06 eV (Refs. 68,69 and 114). Piacentini (Ref. 115) estimates the band gap of LiF to be 14.5 eV. This value is refined in Ref. 66 to 14.2 ± 0.2 eV. Shirley *et al.* (Ref. 65) communicate 14.1 ± 0.1 eV from the dissertation of Himpfel.
- ¹¹⁷Let $N_{\mathbf{A}}$ denote the number of rows of the square matrix \mathbf{A} . Then, specifically for the CO-ADC(2) approximation in terms of Bloch orbitals (17), (18), and (56), a single matrix times vector operation requires $N_{\text{flops}} = 2\{N_{\mathbf{F}(\vec{k})}^2 + (2N_{\mathbf{F}(\vec{k})} + 1)[N_{\mathbf{K}^+(\vec{k})} + N_{\mathbf{K}^-(\vec{k})}]\} = O(N_{\mathbf{F}(\vec{k})}N_{\mathbf{K}^+(\vec{k})})$ flops. By affixing bar accents to the matrices showing up in the expression for N_{flops} , we immediately obtain the corresponding formula for the number of flops required in the CO-ADC(2,2) approximation for Wannier orbitals (29), (32), and (56).
- ¹¹⁸The number of (block-)Lanczos iterations, necessary to determine the eigenvalues and eigenvectors of the band structure matrix (56) with a given accuracy, is assumed to be the same for a single unit cell and a supercell consisting of two unit cells.
- ¹¹⁹This value for the lattice constant of a LiF crystal is utilized in Ref. 38, 43, and 71 and is told to originate from the book of Wyckoff (Ref. 67). However, a value of 4.0173 \AA is reported therein which is consistent with early and recent experimental values. In order to allow comparison, we adopt the previously used value of 3.990 \AA . Although the deviation is small, it has a quite noticeable influence on the fundamental band gap which decreased by 0.65 eV when changing from 3.918 \AA to 4.026 \AA in a recent density functional theory study at the LDA level (Ref. 73).
- ¹²⁰The threshold for the removal of redundancy in the PAO construction was chosen such that the number of discarded virtual Wannier orbitals per unit cell corresponds precisely to the number of occupied Wannier orbitals per unit cell (Ref. 41).